NMR Studies into the Potential Interactions of Fullerene $C_{60,}$ with Tetraphenylporphyrin and Some of its Derivatives

By

Christopher Otara Obondi

December, 2011

Director of Thesis: Art A. Rodriguez

Major Department: Chemistry

ABSTRACT

The curved π surface of fullerene, C_{60}, shows a tendency to interact with other molecules, making it an interesting target for building supramolecular arrays. The interaction can be relative strong and may even exist in solutions, often leading to stable complexes. An important class of the macrocycles that interacts with fullerenes is the porphyrins. In our study, ^{1}H NMR spectrometric studies have been done to gain information on the nature and the precise interaction site of fullerene 1, with tetraphenylporphyrin, H_2[TPP] 2, and para-substituted tetraphenylporphyrins, $H_2[(p\text{-}X)_4TPP]$, where X= CN and OCH_3 in deuterated chlorobenzene-d_5(CBZ) and toluene-d_8. The porphyrin derivatives have been used to investigate any correlation in the interaction site due to changes in substituent. Relaxation rates of the pyrrole and phenyl hydrogen in the porphyrins were determined at temperatures of 288, 298 and 313 K for all the complexes in the presence and in the absence of fullerene, $C_{60.}$ To study solvent effects on interactions, Toluene-d_8 and chlorobenzene-d_5 solvents were used. Overall, our data indicated

that C_{60} interacted with H_2[TPP] at both the pyrrole and phenyl hydrogen sites however, these intermolecular interaction are not long-lasting in chlorobenzene-d_5.

The porphyrin derivatives showed that the substituents have an effect on which site is preferred for interaction. For the case of H_2[(p-OCH_3)$_4$TPP], that has an electron –donating group, both phenyl and pyrrole hydrogen sites interacted with C_{60} , but preferably at the pyrrole hydrogen at all the three temperatures(283, 298, and 313 K). In the case of H_2[(p-CN)$_4$TPP] with an electron-withdrawing group CN, our data indicates that at lower temperature there is a noticeable, but slight preference for the interaction of C_{60} at pyrrole site but is quickly destroyed with an increase in temperature.

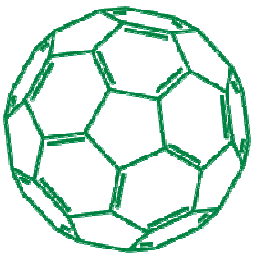

1 C_{60}

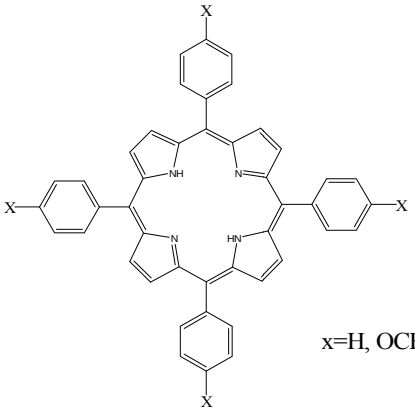

x=H, OCH_3, CN

2

NMR Studies into the Potential Interactions of Fullerene C_{60}, with Tetraphenylporphyrin, H_2[TPP] and some of its Derivatives.

A Thesis

Presented To

The Faculty of the Department of Chemistry

East Carolina University

In Partial Fulfillment

of the Requirements for the

Degree Master of Science

by

Christopher Otara Obondi

December, 2011

NMR Studies into the Potential Interactions of Fullerene, C_{60} with Tetraphenylporphyrin, H_2[TPP] and some of its Derivatives

by

Christopher Otara Obondi

APPROVED BY:

DIRECTOR OF THESIS: _____

(Art A. Rodriguez, PhD)

COMMITTEE MEMBER: _____

(Colin Burns, PhD)

COMMITTEE MEMBER: _____

(Yu Yang, PhD)

COMMITTEE MEMBER: _____

(QUN LU, PhD)

CHAIR OF THE DEPARTMENT OF CHEMISTRY:

_____

(Ricky P. Hicks, PhD)

DEAN OF THE GRADUATE SCHOOL:

_____

(Paul Gemperline, PhD)

ACKNOWLEDGMENTS

I would like to acknowledge the support of my research advisor, Dr. Art A. Rodriguez, who has contributed immensely to this project. From the early stage of the problem identification, right through the research work, and during the write up of this thesis, his encouragement, support and guidance has been fundamental to the successful completion of this project. It has been both a rewarding and pleasurable experience. I would like to extend my thanks to members of my thesis committee, Dr. Colin Burns, Dr. Yang, and Dr. Qun Lu for their time and suggestions. Many thanks are due to the Department of Chemistry, East Carolina University for the moral and financial support; this I greatly acknowledge. Last but not the least, I would like to thank the staff and graduate students of the Department of Chemistry, who made my two-year stay in East Carolina University an enjoyable experience.

TABLE OF CONTENTS

LIST OF TABLES

LIST OF FIGURES

LIST OF ABBREVIATIONS

NMR	Nuclear magnetic resonance
CBZ	Chlorobenzene
H_2[TPP]	Tetraphenylporphyrin
Sfrq	Spectrometer frequency
AT	Acquisition time
Sw	Spectral window
Tpwr	transmittance power
Pw	90º pulse width
p1	180º pulse width
d1	delay time

CHAPTER I

INTRODUCTION

Porphyrins and fullerenes have been found to spontaneously be attracted to each other.[1] This newly recognized supramolecular recognition element, the attraction of the curved π - surface of the fullerene to the center of the flat pi- surface of a porphyrin, is possibly due to π- π and n- π electron interactions. This phenomenon is in contrast to the traditional paradigm which requires the matching of a concave host with a convex guest.[2]

During the past few decades, the intermolecular interaction of porphyrins and fullerenes has been studied extensively. Due to their potential applications in processes of molecular recognition,[3-8] photosynthesis,[9-13] photovoltaics,[14-20] energy transfer,[21-29] and electron transfer[30-40] porphyrin-fullerene complexes have attracted a great deal of attention. Of particular interest is the development of tetraphenylporphyrin-appended silica stationary phases for the chromatographic separation of fullerenes as illustrated below in Figure 5(a). With columns of these materials, Meyerhoff has reported that their selectivity is superior to the commonly used "Buckyclutcher"[41] and "Buckyprep" columns [42-43] shown below in Figure 1(b). The basis of the separation is proposed to be π- π interaction between zinc tetraphenylporphyrin and the fullerene.[44]

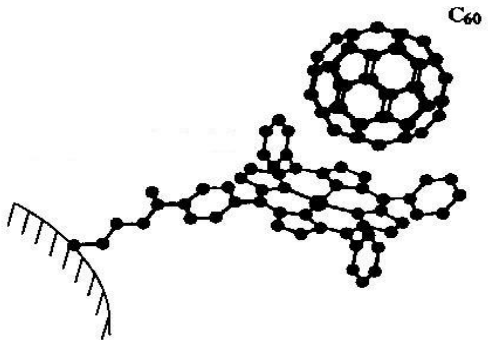

(a)

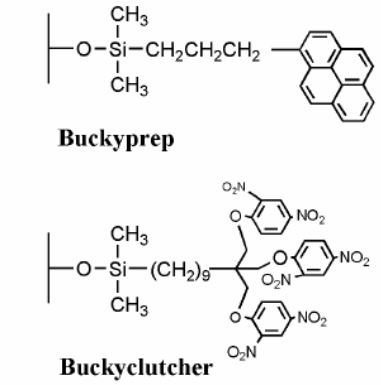

(b)

Figure 1. (a) Structures of immobilized Zinc (II) tetraphenylporphyrin (Zn[TPP]) and buckminsterfullerene(C_{60}); (b)"Buckyclutcher" and "Buckyprep" chromatographic columns.

The π-π interactions are non-covalent interaction between organic compounds containing aromatic moieties often dependent on one being more electron rich and the other electron poor. The arrangement of the five- and the six-member rings in C_{60} leads to its spherical shape. As illustrated below in Figure 2(a), the five-member rings are attached to the sides of six-member rings, each carrying three alternate π-bonds in such a way that none of the π-bonds are in the 6,6-

ring junctions and not in 5,6-ring junction. This kind of structure is energy-minimized and the surface is curved . The π-bonds are bent on the curved exterior surface of C_{60} as shown in Figure 2 (b).

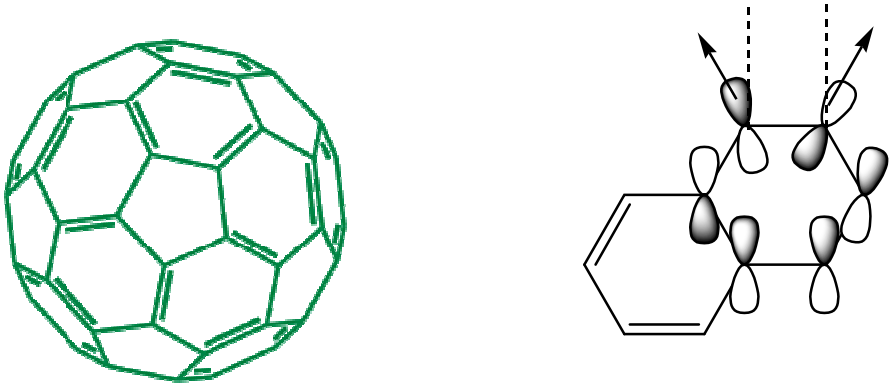

(a) (b)

Figure 2. (a) Three-dimensional structure of C_{60} (b) bent.π-bonds on the surface of C_{60}

As shown in Figure 2 (a) above the double bonds are exocyclic to the 5-membered rings. This means that all the 5,6-ring junctions are single bonds, since a double bond on a 5-membered ring is energetically unfavorable. Thus, all the 6-membered rings have three double bonds each and delocalization is unfavorable. On the other hand, each 5-member ring has to contend with 5-electrons each, one short of aromatization and hence these rings are highly electron – deficient.

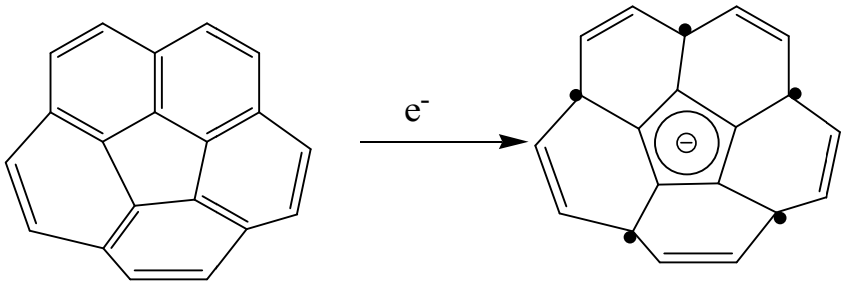

Figure 3. Addition of an electron brings in aromaticity to a pentagonal ring

Overall, the strong electron-deficient character coupled with the three-dimensional symmetrical shape of the C_{60} sphere favors π-π and π-n interactions with electron-rich molecules such as porphyrins, pthalocyanines, etc.

The close association of a fullerene and a porphyrin was first recognized in the molecular packing of a crystal structure of porphyrin-fullerene assembly containing a covalent fullerene-porphyrin conjugate as shown in Figure 4 below.[4]

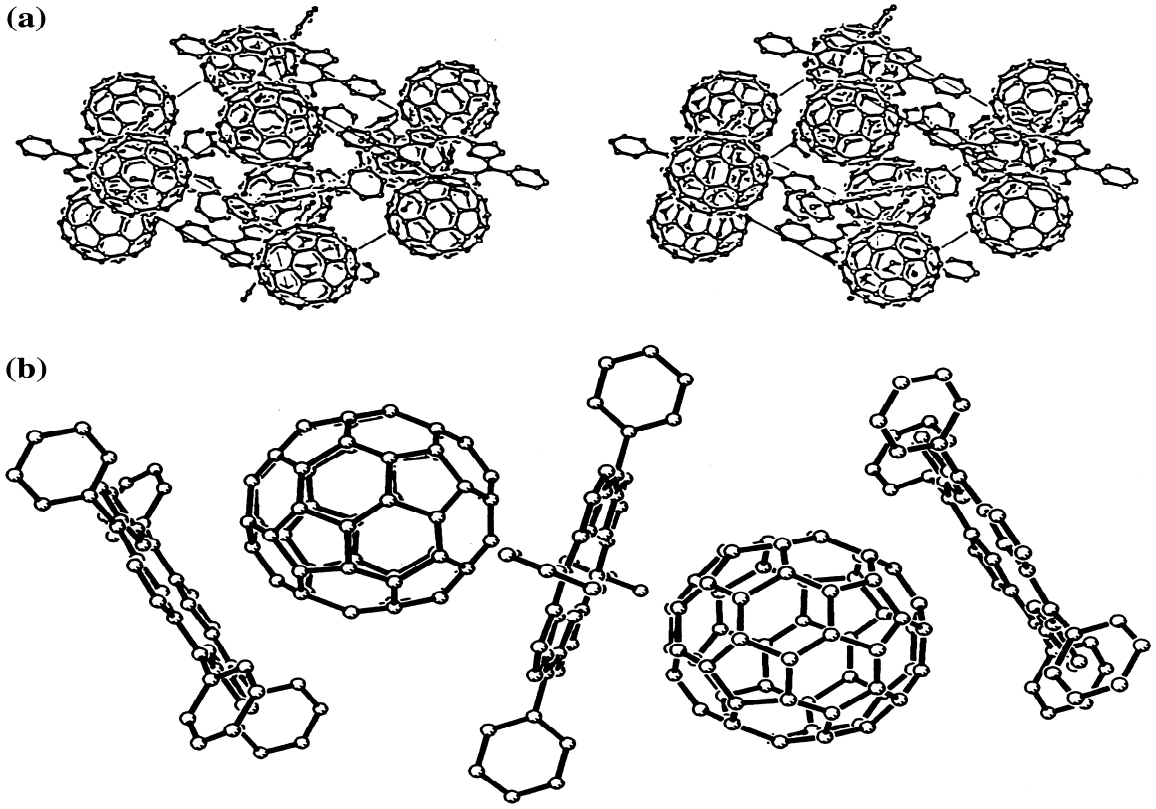

Figure 4. (a) Stereoview of packing diagram for H_2[TPP].C_{60}.3 toluene, (b) A fragment of porphyrin/C_{60} chain.[4]

In the crystal structure of this species, C_{60} was found to be centered over the porphyrin with electron-rich 6:6 ring-juncture C-C bonds in close approach to the plane of the porphyrin core at an average distance of 2.75 Å, shorter than separations of familiar π-π interactions. The closest atom to- atom contacts were from the two 6:6 fullerene carbon atoms to the porphyrin N atoms. They ranged from 3.09 to 4.74 Å. The phenyl carbon atoms of the porphyrin were all at distances >4.0 Å from fullerene carbon atoms, indicating that the ortho C-H bonds do not participate significantly to the association. The angle between the porphyrin planes is 45.2°. The remaining exposed surface of C_{60} was solvated by the methyl groups of lattice toluene, the methyl carbon to fullerene carbon distances lying in the range 3.39-3.59 Å. The closest carbon-to-carbon atom distance between fullerenes in adjacent chains is 3.37 Å. The interaction that is shown to exist in solid state is also shown to extend to solutions, often leading to stable complexes.

In our study, ^{1}H NMR relaxation studies have been done to gain information on the nature and the precise interaction site of fullerene 1, with tetraphenylporphyrin, H_2 [TPP] 2, and para-substituted tetraphenylporphyrins, H_2[(p-X)$_4$TPP], where X= CN and OCH_3 in deuterated chlorobenzene-d_5(CBZ) and toluene-d_8. The porphyrin derivatives have been used to investigate possible interactions with C_{60}, to investigate any correlation in the interaction site due to changes in substituent, and to probe potential solvent effects on intermolecular interactions. Relaxation rates of the pyrrole and phenyl hydrogen in the porphyrins, as shown in Figure 5(a) were determined at temperatures 288, 298 and 313 K for all the complexes in the presence and in the absence of fullerene. In addition, correlation times, τ_c, for these hydrogen were calculated. Possible interaction sites were determined by looking at the difference in relaxation rate, R_1, and correlation time, τ_c, due to the presence and absence of the C_{60} molecule.

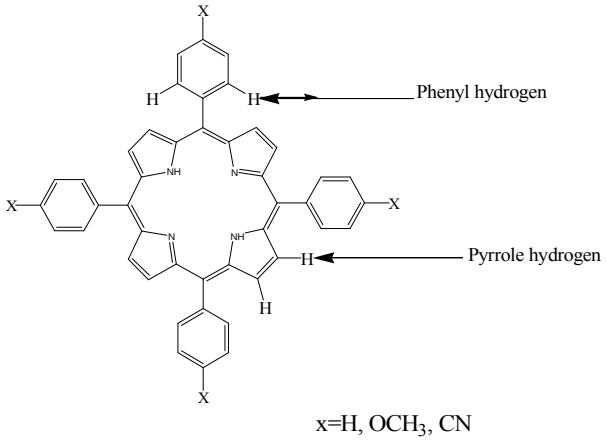

(a)

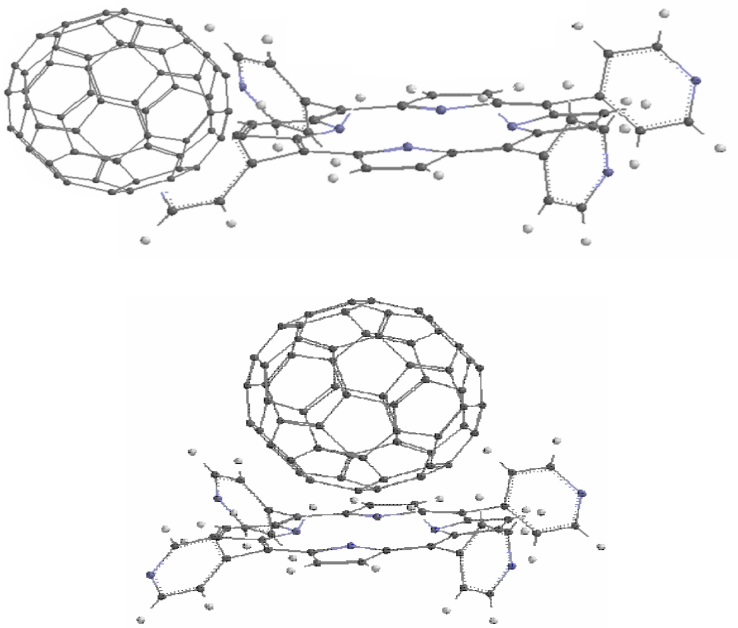

(b)

Figure 5. (a) Structure of H_2[TPP], and Para-substituted tetraphenylporphyrins, H_2[(p-X)$_4$TPP],(b) Possible interaction sites of H_2[(p-X)$_4$TPP] and C_{60}

Objectives of the study

To employ dynamic NMR measurements to study potential interaction sites of fullerene C_{60} with tetraphenylporphyrin, H_2[TPP], and para-substituted tetraphenylporphyrins, H_2[(p-X)$_4$TPP], where X = CN and OCH_3 in deuterated chlorobenzene-d_5(CBZ) and toluene-d_8. A second objective was to determine if there is a preferred site of interaction on the porphyrin based on substituent effects of an electron donating (X = OCH_3) or electron withdrawing group (X = CN). A third objective was to determine the energy of activation of the interactions between C_{60} and the various tetraphenylporphyrins. A fourth objective was to probe whether solvent molecules affect the interaction between C_{60} and the tetraphenylporphyrin, H_2[TPP], and para-substituted tetraphenylporphyrins, H_2[(p-X)$_4$TPP].

CHAPTER II

THEORY

2.1 Basic NMR theory

Nuclear magnetic resonance (NMR) spectroscopy involves the magnetic energy of nuclei when placed in a magnetic field. Fields of appropriate strength cause transitions between nuclear energy levels occur. These fields have a frequency in the radiofrequency (RF) region of the spectrum. The nuclear spin quantum number (I), which may take values of 0, 1/2, 1, 3/2, etc., in units of $h/2\pi$, is the nuclear property that is responsible for the NMR phenomenon and its value for a given nucleus is dependent on its mass and atomic numbers.

Nuclei of certain natural isotopes of the majority of the elements possess intrinsic spin or angular momentum. A fundamental postulate of modern physics is that the total angular momentum , P, of an isolated nucleus has total magnitude that takes only discrete values:[45]

$$P = \hbar[\, I\,(\, I + 1)]^{1/2} \qquad (1)$$

where $\hbar$ is the reduced Planck's constant, $h/2\pi$, I is the nuclear spin quantum number, which takes the value of 1/2, 1, 3/2, and so on. For ^{1}H, I the value is 1/2. Angular momentum exhibits a vector characteristic, therefore, its full description takes into account its magnitude and direction. The directional properties of P are given by the magnetic spin quantum number m_I. According to the principles of quantum mechanics, a nucleus having a spin quantum number of I will have 2I + 1 orientations ranging in values from: +I, I-1, I-2, ⋯, ъ -I.

Since angular momentum of the nucleus, P, is quantized its energy is also quantized. In the absence of an external magnetic field, all the energy levels are degenerate. In the presence of a uniform magnetic field, B_0 the spinning nucleus will produce a magnetic dipole moment which is also quantized and the energy levels lose their degeneracy. The magnitude of the nuclear magnetic dipole moment is given [46]

$$\mu = \hbar g_N \mu_N P \qquad (2)$$

where μ_N is nuclear magneton, its value is 5.05095×10^{-27} J T^{-1}, g_N is the nuclear g-factor, which is a constant for a given type of isotope. For ^1H, g_N is 5.585. Usually the magnitude of the spin magnetic moment is expressed in terms of the magnetogyric ratio, γ.

$$\mu = \gamma P \qquad (3)$$

Substituting P, as given by equation (1) into equation (3), gives the following equation:

$$\mu = \frac{h}{2\pi} \gamma [I (I + 1)]^{1/2} \qquad (4)$$

Equation (4) shows that the magnitude of the spin magnetic moment is quantized. Its directional properties (orientations) are also quantized and are given by the quantum number, m_I. A nucleus with spin quantum number I may lie in (2I+1) different orientations relative to the nuclear axis. Its spin state will split into (2I+1) energy levels. For ^1H, with I = ½, there will be two spin states which are assigned m_I values of ½ and – ½.

When ^1H nuclei are placed in an external magnetic field, the nucleus's own magnetic field, caused by nuclear spin, can align either with or against the external field. When the nuclear spin generates a local field in the same direction as the external field, then this spin state

is assigned a magnetic spin quantum number, m_I (+1/2), and the spin is said to be "aligned". When the nucleus creates a local field in the opposite direction of the external field, the nucleus magnetic spin quantum number m_I is assigned a value of -1/2; and the spin is said to be "opposing" the field. The nuclei with aligned spin are of lower energy than the nuclei with opposing spin. This identifies the energy difference between the separate spin states as shown in Figure 6 below.

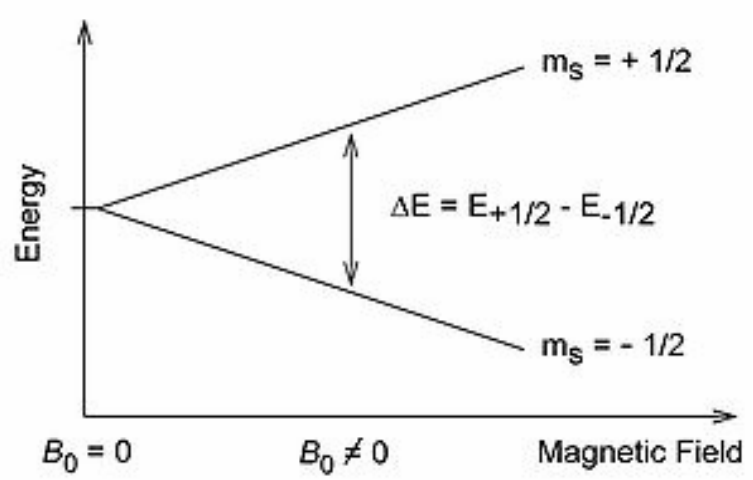

Figure 6: Energy difference, ΔE between ^{1}H spin states in magnetic field B_0.

When the applied magnetic field is assigned the z direction, the projection of the magnetic moment on this z axis will be given by equation (5):

$$\mu_Z = \frac{h}{2\pi} \gamma m_I \quad (5)$$

Its energy is then given by:

$$E = - \mu_Z B_0 = - \frac{h}{2\pi} \gamma m_I B_0 \quad (6)$$

Transitions between the energy levels will occur when Δm_I satisfies the condition of ± 1. Therefore, the energy change upon a transition is given by:

$$\Delta E = \frac{h}{2\pi} \gamma B_0 \quad (7)$$

The frequency, υ_0 of radiation that can induce a transition between adjacent levels is given by

$$\upsilon_0 = \frac{\Delta E}{h} = \frac{\gamma B_o}{2\pi} \quad (8)$$

or

$$\omega_0 = 2\pi\upsilon_0 = \gamma B_0 \ (\text{rad sec-1}) \quad (9)$$

where ω_0 is known as angular frequency.

At equilibrium, the nuclei maintain a Boltzmann distribution among the spin states, hence one expects more nuclei to reside in the lowest energy states. For a system of spin -1/2 nuclei a Boltzmann distribution would give:

$$\frac{N_u}{N_l} = e^{-\Delta E/kT} \quad (10)$$

Where N_u and N_l are the numbers of nuclei in the upper and lower energy states respectively, ΔE is the energy separation, k is the Boltzmann constant, and T is the absolute temperature.

After the disruption of this distribution by absorption of radio frequency energy, the nuclear spin system will revert back to equilibrium with the "lattice" (its surroundings) by a first-order relaxation process characterized by a time T_1, called the spin-lattice relaxation time.[47]

2.1.1 Spin-lattice relaxation

It has been shown that a torque exerted on a magnetic moment by an applied magnetic field will cause the magnetic moment to precess about the direction of the field with a frequency given by[48]

$$\omega_0 = \frac{\gamma B_O}{2\pi} \quad \text{or} \quad \omega_0 = \gamma B_0 \ (\text{rad sec}^{-1}) \tag{11}$$

The precession of the magnetic moment of a nucleus is shown in Figure 7(a). Energy will be absorbed only when the radio frequency (υ_{rf}) of the second magnetic field (B_1), which is perpendicular to B_0 (i.e., in the xy plane) as depicted in Figure 7(a) are equal i.e. $\upsilon_{rf} = \upsilon_0$. This absorption is called "resonance". On absorption of energy from B_1, the magnetic moment will tip to a different angle θ, but its precession frequency will remain the same.

The discussion above is for a single nuclear magnetic moment, but we typically study a large collection of identical nuclei referred as an ensemble. Figure 7(b) illustrates the precession of moments of nuclei with $I = \frac{1}{2}$ and all moments precesses at the same frequency. There is a directional reference along the magnetic field B_0 which has been traditionally assigned the z direction. Based on Boltzmann distribution, at equilibrium more nuclei will be aligned in the direction of B_0 than opposing it. Consequently, when an ensemble of nuclei are placed in a magnetic field, this will result in a net magnetization M oriented along the field direction given by:[49]

$$M = \frac{N\gamma^2 h^2 I(I+1)B_O}{8\pi^2 kT} \tag{12}$$

where N is the nuclei number density.

When M is perturbed from its equilibrium value (M_0) by applying a second magnetic field (B_1) perpendicular to B_0, the equation of motion of this non-equilibrium magnetization, after B_1 has been turned off and in the absence of interactions between spins or with the surrounding, is simply given by

$$\frac{dM}{dt} = \gamma(M \times B_O) \qquad (13)$$

From the above equation states, M will precess about the field direction with a frequency given by $\omega_0 = \gamma B_0$ (Larmor equation). In NMR, it is a common practice to view M from a reference frame rotating at the Larmor frequency which simplifies the characterization of its motion. In the rotating frame, the magnetization appears to be a static vector with components both parallel (M_Z) and perpendicular (M_X, M_Y) to the applied field.

Figure 7. (a) Precession of μ about B_0; (b) Precession of an ensemble of nuclei with I=1/2

The situation described above represents a non-equilibrium population of energy states. At equilibrium, components M_X and M_Y of M are equal to zero. Because of the natural processes that cause nuclei to exchange energy with each other and their environment, their environment is considered to be a constant temperature reservoir (lattice) having infinite heat capacity. The coupling of spins to the lattice permits the exchange of energy, allowing an

approach back to an equilibrium population of energy states, and therefore returning M_Z to its equilibrium value, M_0. Bloch showed that this could be treated as a first order rate process and is expressed by the following equation:[50]

$$\frac{dM_Z}{dt} = -\frac{1}{T_1}(M_Z - M_0) \tag{14}$$

where T_1 is called the spin-lattice relaxation time. The integration of equation (14) gives;

$$M_z(\tau) - M_0 = (M_z(0) - M_0)e^{\tau/T_1} \tag{15}$$

where $M_Z(\tau)$ is the value M_Z at different delay times of τ, M_0 is the value M_Z at equilibrium.

The explanation for the relaxation of the M_Z component of the magnetization M is as follows. In mobile liquids, the microscopic environment of a spin is exposed to rapid changes due to the translational and orientation motions of molecules in the sample which lead to random fluctuations of the magnetic fields experienced at the nucleus. In these rapid fluctuations, there will be Fourier components at the Larmor frequency which will couple different energy states and thus, allow the relaxation of M_Z to its equilibrium value.

There are various independent mechanisms which couple the spins to the lattice and thus promote spin-lattice relaxation. The relaxation rate for a particular nucleus in a specific chemical environment will depend upon which mechanisms are operating in this environment. In later sections of this chapter, a brief review of the more important mechanisms present of the hydrogen being studied in tetraphenylporphyrin, (H_2[TPP]) will be discussed.

2.2 Relaxation mechanisms

Spin-lattice relaxation, as discussed in the previous section will only occur if there is a physical coupling between the resonant nuclei and the lattice by which energy exchange can take place. The following types of interactions are known to couple the nuclei to the lattice:

(a) Quadruple interaction

(b) Chemical shift anisotropy

(c) Scalar coupling

(d) Spin rotation

(e) Magnetic dipole-dipole

Each of the above mechanisms contributes to a different degree to the overall relaxation process. However in the tetraphenylporphyrin H_2[TPP] system only the magnetic dipole-dipole interactions are operative. Due to the very high value of the hydrogen gyromagnetic ratio, g, the dipole-dipole interactions will dominate the relaxation process.[45] A brief description of the above mentioned relaxation mechanism is given below.

2.2.1 Quadrupole interaction mechanism

Nuclei with spin I > ½ have an electrical quadrupole moment, which is caused by the non-spherical charge distribution inside the nucleus. The coupling between this electric field and the electric field gradient generated by the molecular environment in which the nucleus is situation provides an effective way towards relaxation of this type of nucleus. The rate of quadrupole relaxation, R_1^Q assumes extreme narrow conditions and is given by the expression: [51]

$$R_1^Q = \left(\frac{1}{T_1}\right) = \frac{3}{40}\left[\frac{(2I+3)}{I^2(2I-1)}\right]\left[\frac{e^2Qq}{\hbar}\right]^2 \tau_0 \qquad (16)$$

Where I is the spin of the quadrupole nucleus, ($e^2Qq/\hbar$) is the quadrupole coupling constant (in rad.sec^{-1}) and τ_0 is the rotational correlation time. It is worth noting that in the current study the nuclei of interest (C and H) have spin values of ½ hence quadrupole relaxation mechanism pathway is non-existent.

2.2.2 Chemical shift anisotropy

The local electromagnetic field experienced by the nucleus is given by

$$H_{loc} = H_0 - \sigma H_0 = H_0(1 - \sigma) \tag{17}$$

where σ and H_0 are the shielding factor and static field respectively. If a molecule is anisotropic, σ will vary in direction and different chemical shifts will be observed along different molecular axes. Since motions in non-viscous liquids are rapid, one only sees an average shield, $= (2\sigma_\perp + \sigma \|)/3$. However, anisotropy in σ will result in an orientation dependence of the instantaneous local magnetic field at the nucleus and modulation of coupling between H_{loc} and the relaxing nucleus by molecular rotation will furnish a pathway for relaxation. The expression characterizing the relaxation rate is:

$$R_1^{CSA} = \left(\frac{1}{T_1}\right)^{CSA} = \frac{2}{15}\gamma^2 H_0^2 (\sigma\_\| - \acute{o}\_\perp)^2 \tau_\theta \tag{18}$$

Where $\sigma\_\| \; and \; \sigma\_\perp$ are components of the shielding tensor parallel and perpendicular to the axis of symmetry and τ_θ is the correlation time for tumbling motion. It has been found that, in the presence of other relaxation mechanisms and at moderate field strengths, the CSA contribution to the overall relaxation rate is very small and can be neglected.[51]

2.2.3 Scalar coupling

The scalar (spin-spin) coupling mechanism is similar to the dipolar process. The effect of scalar coupling relaxation on T_1 is significant only if the two interacting nuclei have very close frequency. It's very rare for that this condition to be met. It takes place for instance for Br-79 (75.29 MHz with B_1=7.06 T and) Carbon-13 (75.56 MHz with B_1=7.06 T) which are very close in frequency. Scalar relaxation is more important for the T_2 relaxation as with this mechanism the quadrupolar nuclei can broaden lines significantly on nuclei that are coupled to it.

2.2.4 Spin-rotation mechanism

Spin rotation is known in some cases to significantly contribute to nuclear relaxation. The molecular rotation in a medium generates a magnetic field at the nucleus of interest. The magnitude of which depends on the angular velocity (or alternatively on the angular momentum, J). Collisions of the molecule with its neighbors will cause a change in the field at the nucleus. The randomly fluctuating magnetic field due to the collisions will cause relaxation of the nuclear spin system. The Magnitude of this interaction is characterized by the spin-rotation coupling constant (τ_J) and the rate of relaxation for a spherical molecule is given by:[49]

$$R^{SR} = \left(\frac{1}{T_1}\right)^{SR} = \frac{2IkT}{\hbar^2} C^2 \tau_j \qquad (19)$$

Where C equals ($2C_\perp + C_\parallel$), I is the molecule moment of inertia and τ_j is the correlation time , decay time of the angular momentum correlation function (17). The above mechanism is not applicable to the system of interest in this study as the concentration of molecules is very dilute precluding interaction.

2.2.5 Magnetic dipole-dipole relaxation

Proton, ^{1}H, spin-lattice relaxation can be expressed as the sum of intra and inter-relaxation. This relationship is demonstrated below by equation (20).[52]

$$\frac{1}{T_1} = R_1 = R_1^{DD}(\text{intra}) + R_1^{DD}(\text{inter}) \tag{20}$$

T_1 is measured by NMR and R_1 is simply the inverse of T_1. In cases where the mole fraction of a solute is as small as $1.299\text{x}10^{-5}$ and when working in deuterated solvents, the inter-relaxation becomes negligible. When dipole-dipole relaxation is due to hydrogen-hydrogen interaction the above equation can be reduced and rewritten as

$$\mathrm{R_1} = \mathrm{R_1}^{\mathrm{DD}}(\text{intra}) = \left(\frac{\mu_o}{4\pi}\right)^2 \left[\left(\frac{2}{3}\right)\frac{\gamma_H{}^4\hbar^2}{r_{AB}^6}\right]\eta_s\tau_c \tag{21}$$

where γ_H = $2.6752\text{x}10^4$ rad $G^{-1}s^{-1}$ gyromagnetic ratio, r_{AB} is the proton-to-proton distance of the interacting nuclei, n_s is the number of interacting nuclei, μ_0 is the vacuum permeability constant ($12.57 \times 10^{-6}\ \mathrm{j.s^2/C^2.m}$) and τ_c is rotational correlation time.. The rotational correlation time is the period of time necessary for a specific nuclear site to undergo reorientation (i.e. movement) to a new position which is different by about 54°.

Once relaxation rates have been determined, the rotational dynamics at a specific molecular site can be analyzed since the correlation time can be expressed by equation (22).

$$\tau_c = \left(\frac{\mu_o}{4\pi}\right)^2 \left(\frac{2}{3}\right)\left(\frac{r_{AB}^6}{\hbar^2\gamma_H^4}\right) R_1^{DD}(\text{intra})\eta^{-1} \tag{22}$$

Once relaxation rates have been determined, the rotational dynamics at a specific molecular site can be analyzed since the correlation time can be expressed by equation 22. A straight forward method of analyzing possible complexation at a site is by determining the variation of the relaxation rate of the host in the presence and absence of a guest molecule. The changes in R_1 (i.e. ΔR_1) can also be used to determine the site of complexation. The first step in determining ΔR_1 is measuring the relaxation rate of particular nuclei in the host in CBZ (deuturated chlorobenzene), $R_1(A)$, followed by measuring the relaxation rate of the same nuclei after the introduction of a guest, $R_1(B)$. The difference in measurements can then be used to acquire the necessary information.

$$\Delta R_1 = R_1(A) - R_1(B) \tag{23}$$

$R_1(A)$ is the value obtained when only host is present in the solution while $R_1(B)$ is the relaxation rate obtained for the host in the presence of the guest solute. Since the relaxation rates are obtained with equivalent mole fractions and in the same solvent environment, the observed difference in the relaxation rates, ΔR_1 can be correlated to dynamical changes due to intermolecular complexations. The energy can be calculated once the rotational correlation times have been obtained at several temperatures.

2.3 Arrhenius fit of correlation times

Once the correlation times τ_c is determined from the dipole-dipole relaxation rates, as shown in equation 22, correlation times were related to activation energy, E_a, using equation (24);

$$\tau_c = \tau_0 e^{\frac{-E_a}{RT}} \tag{24}$$

where τ_c is correlation time,, τ_o is the inertial or 'free rotor' correlation time, is an experimentally obtained parameter which is often associated with the rotational motion in pure 'slip' limit. The activation energy, E_a, is the amount of energy necessary for the portion of the molecule, containing the hydrogen in question, to undergo rotation to a new position that is approximately 54° different from a previous location. Equation 24 can be modified to become equation 25 by taking natural log of both sides.

$$\ln(\tau_c) = \ln(\tau_0) - \frac{E_a}{RT} \tag{25}$$

A plot of $\ln(\tau_c)$ versus T^{-1} (K) will generate a line with a slope equal to $-E_a/R$. Once E_a is determined for every studied proton, the energy of complexation at each site can be determined. Both change in relaxation rates, ΔR and activation energy, E_a for every studied proton provides information regarding complexation at a site. Both are important since each provides a slightly different type of information. Ea give the energy requirements for rotational motion (low values indicate low energy barrier for rotation and vice versa) and τ_C gives a "raw" indication of which hydrogen site is moving faster. The τ_c values can range from 0.1 ps in methyl groups to 15 ps in larger molecules such as C_{60}.

2.4 Experimental measurement of the spin-lattice relaxation Rate

The measurement of spin-lattice relaxation time can be done by using the standard inversion-recovery pulse sequence (i.e. D_1-π-τ-π/2) where π is a 180° pulse, π/2 is a 90° pulse, τ is a delay which is under the control of the operator. This method is illustrated in Figure 3. In Figure 2, M_0 is the Boltzmann equilibrium value of magnetization M. The magnetization is initially aligned along the z axis and is inverted to -z by the π pulse. After a short delay, the

magnetization will not have recovered to any significant extent and the π/2 pulse will rotate it to the -y axis. Since the instrument detector is phase sensitive and configured to detect along the y axis, the signal, after Fourier transformation, will appear inverted compared to a signal generated by a π/2 pulse of the equilibrium magnetization. If, in a separate experiment, we wait a little longer before applying the π/2 pulse, the magnetization would recover to a point just below the origin. Now a π/2 pulse will move the magnetization to the -y axis, producing a smaller but still negative signal. If we wait longer periods of time, the magnetization will pass through the origin, and the π/2 pulse will generate +y magnetization and a positive signal will be produced. If we wait long enough between the pulses, the magnetization will eventually recover to its equilibrium value of M_0.

The z component of magnetization as a function of τ is given by the following equation [52]

$$M_z(\tau) - M_0 = (M_z(0) - M_0) \exp(-\tau/T_1) \qquad (26)$$

where $M_Z(\tau)$ is the signal intensity at various τ values, M_0 is the signal equilibrium value, and $M_z(0)$ is the signal intensity immediately after the 180° pulse (i.e., no delay time before the 180 and 90 pulse). At $\tau = 0$, $M_z(0) = -M_0$. Substitution of this relation into equation (26), followed by rearrangement, gives equation (27):

$$\mathrm{Ln}(M_0\text{-}Mz(\tau)) = \mathrm{Ln}2 + \mathrm{Ln}(M_0) - \tau/T_1 \qquad (27)$$

The experimental relaxation rate, R_1 ($1/T_1$) is obtained from a linear fit of $\mathrm{Ln}(M_0\text{-}M_z)$ versus τ.

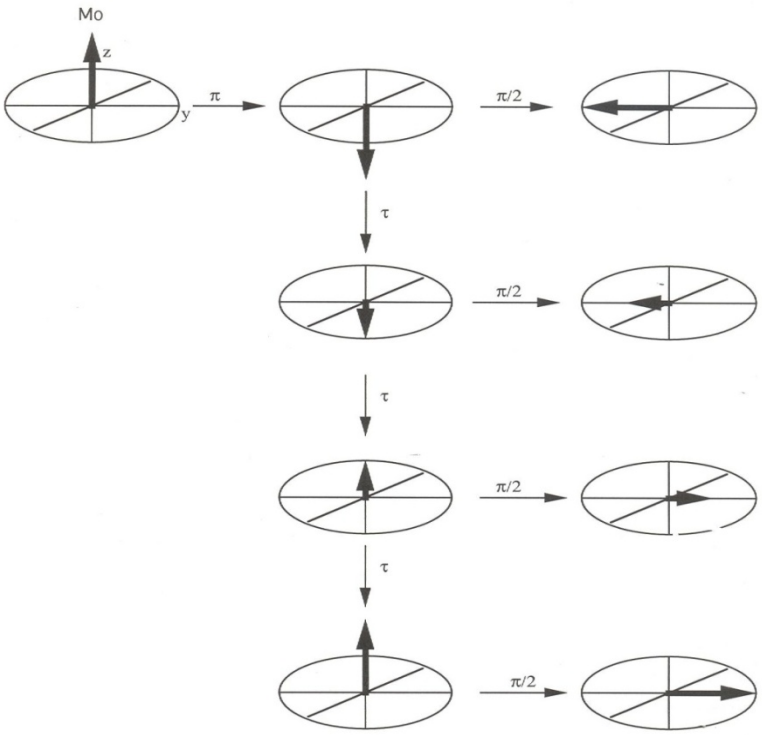

Figure 8. Vector diagram of the inversion –recovery pulse sequence

CHAPTER III

EXPERIMENTAL

3.1 Chemical and materials

Fullerene C_{60}, chlorobenzene-d_5 (99.5+ at.% D) and toluene-d_8 were purchased from Acros Organics.[53] Tetraphenylporphyrin H_2[TPP] was purchased from the Aldrich Chemical Company.[54] The derivatives of para- substituted tetraphenylporphyrin derivatives H_2[(p-X)$_4$TPP](X = CN and OCH_3) H_2[TPP] were synthesized as described below.

3.2 Synthesis of para- substituted tetraphenylporphyrin derivatives H_2[(p-X)$_4$TPP](X = CN and OCH_3)

The synthesis of the porphyrins was done by a previous student in our research group and the method used was adapted from the synthesis as reported by *Adler et al.*[55]

The appropriate benzaldehyde was refluxed with pyrrole in propionic acid in a round-bottom flask fitted with a water condenser. After refluxing, the reaction mixture was cooled to room temperature and cold methanol is added. The flask was then chilled in an ice bath while stirring, and crystallization was induced by scratching the sides of the flask with a glass stirring rod. The deep-purple crystals were filtered by vacuum filtration with a Buchner funnel. The flask and crystals are washed with three 0.5-mL portions of cold methanol followed by three 0.5-mL portions of boiling distilled water. The crystals were air-dried on the Buchner funnel. For H_2[(*p*-CN)$_4$TPP], 4-cyanobenzaldehyde was used and for H_2[(*p*-OCH_3)$_4$TPP], 4-methoxybenzaldehyde was used.

3.3 Solvent and sample preparations

Chlorobenzene-d_5 and Toluene-d_8 were received prepackaged in scored glass ampoules and were used as received. Host and guest amounts were initially introduced into toluene-d_8 according to the amounts given below follows:

a. (i) 7.99 mg (0.1299 μmoles) of H_2TPP was dissolved in 1.50 ml of solvent.

(ii) 7 .99 mg (0.1299 μmoles) of H_2TPP and 9.35 mg (0.1299 μmoles) of C_{60} were dissolved in 1.50 mL of solvent.

The solute and solvent amounts produced solution with a mole fraction of $0.1299\ \mu moles$. After preparing these toluene-d_8 solutions, sample precipitation was noticed occurring in H_2[(p-$OCH_3)_4$TPP] and H_2[(p-CN)$_4$TPP] solutions. Therefore, a second more appropriate solvent was sought. After investigating various solvents, chlorobenzene-d_5 was determined to be applicable with all the samples. Solutions of H_2[TPP] and other derivatives were prepared according to the following amounts:

a. (i) 3.87 mg (6.29 μmoles) (of H_2TPP was dissolved in 1.0mL of solvent.

(ii) 3.87 mg (6.29 μmoles) of H_2TPP and 4.53 mg (6.29 μmoles) of C_{60} were dissolved in 1.0 mL of solvent.

b. (i) 4.63 mg (6.29 μmoles) of H_2[(p-$OCH_3)_4$TPP] was dissolved in 1.0 mL of the solvent

(ii) 4.63 mg (6.29 μmoles) of H_2[(p-$OCH_3)_4$TPP] and 4.53 mg (6.29 μmoles) of C_{60} were dissolved in 1.0 mL of the solvent.

c. (i) 4.50 mg (6.29 μmoles) of H_2[(p-CN)$_4$TPP] was dissolved in 1.0 mL of solvent.

(ii) 4.50 mg (6.29 μmoles) of H_2[(p-CN)$_4$TPP] and 4.53 mg (6.29 μmoles) of C_{60} were dissolved in 1.0 mL of the solvent.

Approximately 0.5 mL of each sample was transferred into a 5-mm NMR tube, connected to a vacuum line and thoroughly degassed by several freeze–pump–thaw cycles to eliminate molecular oxygen. The tubes were then sealed under vacuum.

3.4 Instrumental

^{1}H spin-lattice relaxation measurements were made on Varian 300 NMR with field strength of 7.0 tesla. Experiments were conducted at three different temperatures (283, 298, and 313 K). Typical acquisition parameters are listed below:

Table 1. Instrumental parameters for T_1 measurements

Parameter	Value
Sfrq	299.935 MHz
AT	3.7 db
Sw	4000 Hz
Tpwr	60 db
Pw	27 μs
p1	54μs
d1	14s
Nt	76

3.5 Calibration of 90º and 180º degree pulses

Acetone-d_6 chemical reagent was chosen a standard for this calibration of the NMR. Standard regular proton NMR spectrum for the standard was taken and the pulse width (pw) 90 º pulses in microseconds were determined from a well phased spectrum. The pulse width (pw) was varied and peak intensity was measured. Starting with the pw value obtained and a properly phased spectrum, pw was adjusted such that a series of spectra that started in positive, pass through a null at 180^o, became negative. The peak heights were measured to ascertain they were of the same intensity.

3.6 Measurement of relaxation time

All relaxation measurements for the pyrrole and phenyl protons of tetraphenylporphyrin, H_2[TPP], and para-substituted tetraphenylporphyrins, H_2[(p-X)$_4$TPP] were done on Varian instrument operating at 7.0 tesla. Typical ^{1}H NMR spectra of the H_2[TPP], H_2[(p-OCH_3)TPP], and H_2[(p-CN)$_4$TPP] were obtained as shown in Figure 9 , Figure 10, and Figure 11 respectively. The spectra values agreed with those reported by Adler *et al* [55]thus we were able to differentiate the pyrrole and phenyl protons.

The relaxation studies were carried out at three different temperatures (283,298, and 313 K) for each solvent chosen within the melting and boiling points of each solvent. For each proton of interest at the three temperatures, relaxation time measurement was done in triplicate.

All relaxation times were obtained using the standard inversion-recovery pulse sequence (i.e. D_1-π-τ-π/2), where π is a 180° pulse, π/2 is a 90° pulse and τ is the delay time.

Nine delay times were used in the inversion-recovery pulse sequence and the values ranged from 0.0625 s to 16 s times depending on the estimated T_1. A delay time (d_1) of approximately 14 s was used between the transients. Each experiment used 76 transients resulting in an acquisition time of approximately 4 hours.

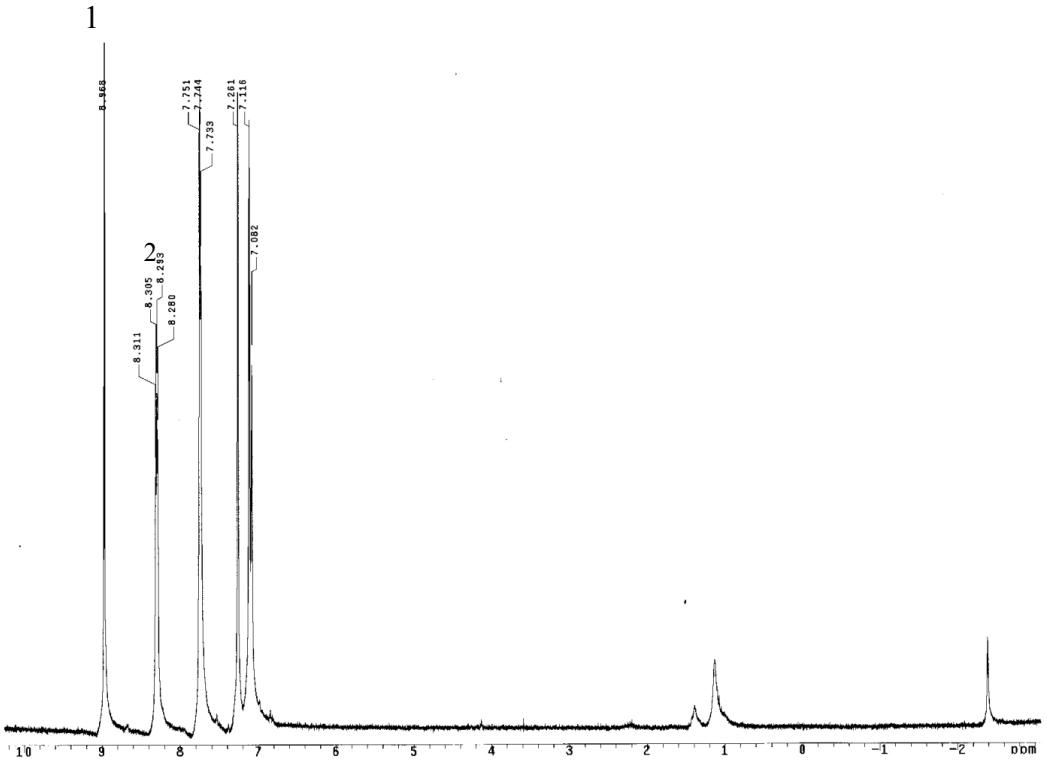

Figure 9. ^{1}H NMR of H_2[TPP] in chlorobenzene-d_5. The peaks at 8.95, 8.31 and -2.5 ppm corresponds to the pyrrole, ortho phenyl and N-H proton respectively.

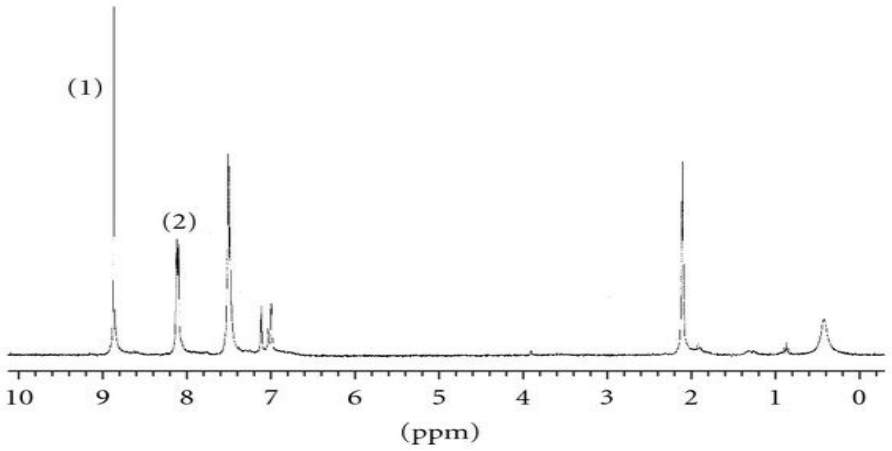

Figure 10. ^{1}H NMR of H_2[(p-OCH_3)TPP] in chlorobenzene-d_5. Peak 1, at about 8.87 ppm, corresponds to the pyrrole hydrogen while peak 2, about 8.11 ppm, corresponds to the ortho hydrogen of the phenyl group.

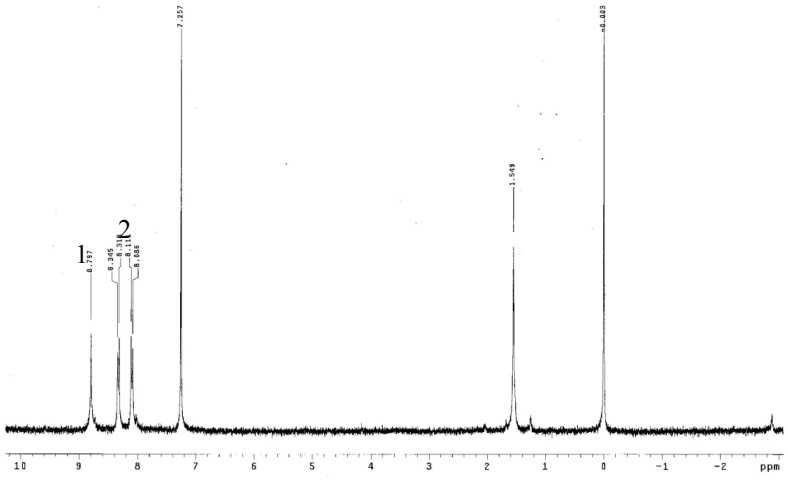

Figure 11. ^{1}H NMR of H_2[(p-$CN)_4$TPP] in chlorobenzene-d_5 Peak 1, about 8.80 ppm, corresponds to the pyrrole hydrogen while peak 2 , at about 8.32 ppm, corresponds to the ortho hydrogen of the phenyl group.

3.7 Statistical Analysis of Data

Ninety percent (90%) confidence limits for relaxation times, R_1 values was determined using equation 27 below. This was especially important because these values provide the basis for telling if the porphyrin and C_{60} are interacting. Confidence limits are calculated according to the equation:

$$\lambda = \frac{\mathrm{t}\,(90\%)\sigma}{\sqrt{\mathrm{N}}} \tag{27}$$

where t(90%) is the statistical "Student t-factor" of 2.353, σ is the standard deviation of the relaxation rates, and N is the number of experiments performed in the set. A value of 0.01 for λ, at the 90% confidence limit, would be interpreted as; "there is a 90% probability that the real or true value is +/- 0.01 of the reported value."

CHAPTER IV

RESULTS AND DISCUSSION

1.1 ^{1}H Relaxation rates and correlation time of pyrrole hydrogen in H_2[TPP] with and without C_{60} in chlorobenzene-d_5

Shown below in column 2 of Table 2 is the relaxation rate, R_1 of the pyrrole hydrogen in the absence of C_{60} for H_2[TPP]. The rate is seen to decrease with increasing temperature. This trend is also illustrated in Figure 12 below and indicates that the dipole-dipole relaxation pathway is becoming less efficient or less effective in relaxing this hydrogen as the temperature increases. The effectiveness of the dipole-dipole pathway is inversely proportional to how fast the dynamic motion is at that molecular site. This is further shown in the correlation time, τ_c. The correlation time is decreasing with increasing temperature indicating that the molecule is undergoing faster dynamics with rising temperature. As the temperature increases, Brownian motion increases and the correlation time decreases.[49]

The fourth column of Table 2 contains the relaxation rate of the same pyrrole proton, but now in the presence of C_{60}. The relaxation rate is also seen to decrease with rising temperature. This also suggests that the pathway is becoming less efficient at relaxing this hydrogen with rising temperature. We also see that the correlation time, τ_c decreasing with rising temperature which again indicates faster molecular motion.

The introduction of C_{60} to the solution does not affect the relaxation rate of this proton appreciatively. One notices from the values that the change in relaxation rate, ΔR are within the experimental error. This indicates that the presence of C_{60} does not lead to noticeable intermolecular interaction at the pyrrole site of H_2[TPP].

The variation of the relaxation rate and correlation time with temperature for this proton is also further illustrated graphically in Figures 12 and 13 respectively. The graphs were obtained through joining the points.

Table 2. ^{1}H Relaxation rates of pyrrole hydrogen in H_2[TPP] with and without C_{60} in chlorobenzene-d_5(CBZ).

T (K)	H_2 [TPP] in CBZ		H_2[TPP] with C_{60} in CBZ			
	R_1 (1/s)	τ_C (ps)	R_1 (1/s)	τ_C (ps)	ΔR_1 (1/s)	$\Delta\tau_C$ (ps)
283	0.581 (0.006)	288	0.571 (0.013)	283	-0.01	-5
298	0.496 (0.016)	246	0.515 (0.010)	255	0.019	9
313	0.434 (0.002)	215	0.432 (0.011)	214	-0.02	-1

Values in parenthesis are error limits at the 90% confidence levels. Each relaxation time, R_1 is an average of three measurements.

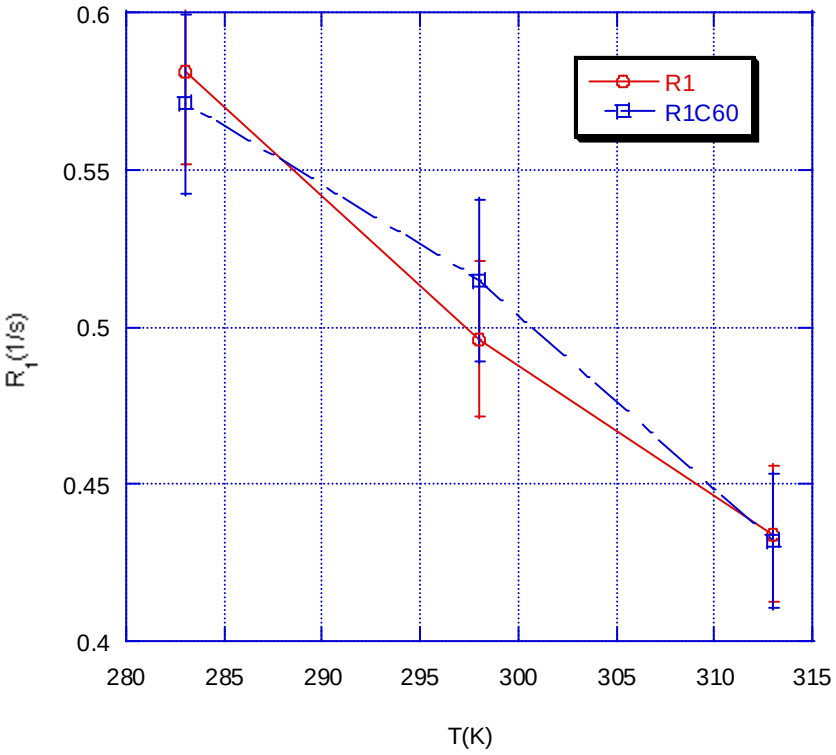

Figure 12. Relaxation rates of pyrrole hydrogen in H_2[TPP] with C_{60}, R_1 (dashed line) and without C_{60}, R_1C_{60}(Solid line) in Chlorobenzene-d_5.The lines on the graph represent connected dots.

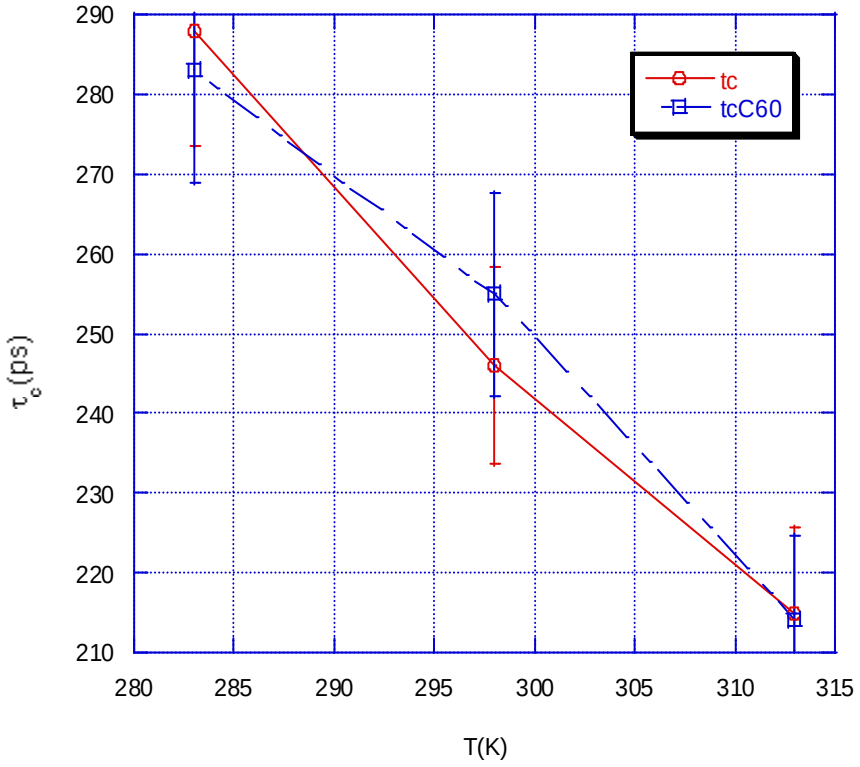

Figure 13. Experimental Correlation times of pyrrole hydrogen in H_2[TPP] with C_{60}, R_1 (dashed line) and without C_{60}, R_1C_{60}(Solid line) in Chlorobenzene-d_5. The lines on the graph represent connected dots.

An Arrhenius fit of $\ln(\tau_c)$ versus T^{-1} (K) as shown in figure 14 generated activation energy, E_a, values of 7.2 and 6.80 kJ/mole for H_2[TPP] without and with C_{60} respectively.

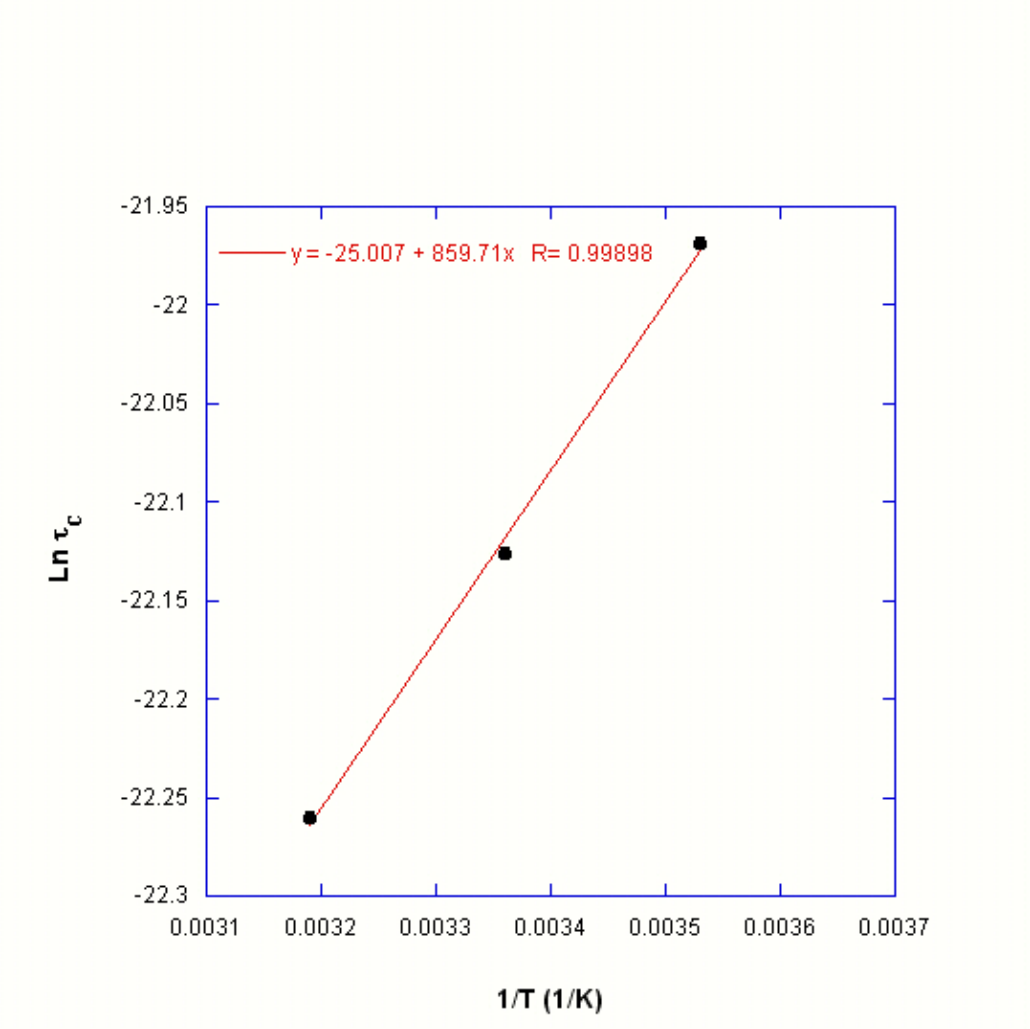

Figure 14. Linear fit of experimental correlation times of the pyrrole protons of H_2[TPP] in neat chlorobnzene-d_5 to obtain activation energy of complexation at the site of interaction.

1.2 ^{1}H Relaxation rates and correlation time of phenyl hydrogen in H_2[TPP] with and without C_{60} in chlorobenzene-d_5

As seen in column 2 of Table 3, the relaxation rate of the phenyl hydrogen in the absence of C_{60}, is seen to decrease with rising temperature indicating that the relaxation pathway is becoming less efficient or less effective. This is further shown in the correlation time, τ_c. One sees that the correlation time decrease with increasing temperature indicated that the molecule is undergoing faster dynamics at this site. Column 4 of the same table contains the relaxation rate

of the same hydrogen upon the introduction of C_{60} into solution. The relaxation rate is seen to decrease with rising temperature. This also suggests that the pathway is becoming less efficient at relaxing this hydrogen. We also see that as the temperature rises, the correlation time decreases, an indication of faster molecular motion.

Again as seen in column 6 of Table 3, the introduction of C_{60} to the solution does not affect the relaxation rate of this proton appreciatively. The values of the change in relaxation rate ,ΔR are within the experimental error an indication that the presence of C_{60} does not lead to noticeable intermolecular interaction at the pyrrole site of H_2[TPP].

The above trends of relaxation rates and correlation times of this proton with respect to temperature are further illustrated in Figures 15 and 16 respectively.

An Arrhenius fit of Ln τ_c versus 1/T illustrated in figure 17 gave values of 6.76 and 6.69 kJ/mole for H_2[TPP] and H_2[TPP] with C_{60}, respectively, suggesting that the energy difference of activation for molecular motion with and without C_{60} are very similar.

Table 3. ^{1}H Relaxation rates of phenyl hydrogen in H_2[TTP] with and without C_{60} in chlorobenzene-d_5 (CBZ)

T (K)	H_2[TTP] in CBZ		H_2[TTP] with C_{60} in CBZ			
	R_1 (1/s)	τ_C (ps)	R_1 (1/s)	τ_C (ps)	ΔR_1 (1/s)	$\Delta\tau_C$ (ps)
283	0.752 (0.032)	106	0.729 (0.084)	103	-0.023	-3
298	0.606 (0.012)	86	0.660 (0.019)	93	0.054	7
313	0.576 (0.008)	81	0.557 (0.010)	78	-0.019	-3

Values in parenthesis are error limits at the 90% confidence limits. Each relaxation time,R_1 is an average of three measurements.

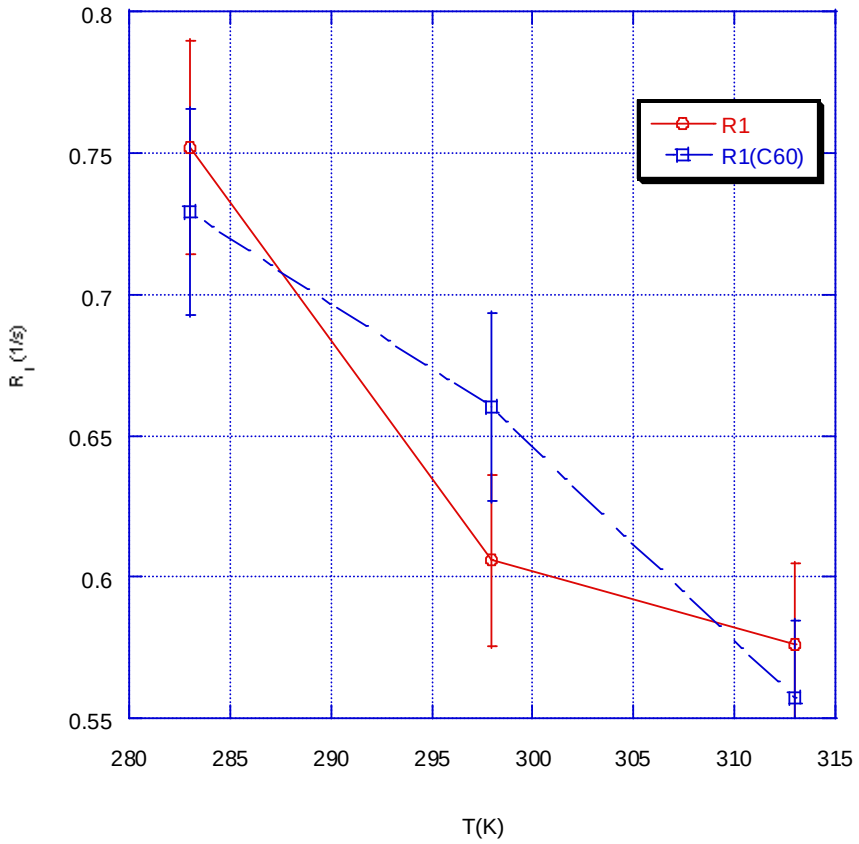

Figure 15. Relaxation rates of phenyl hydrogen in H_2[TPP] with C_{60}, R_1 (dashed line) and without C_{60}, R_1C_{60}(Solid line) in chlorobenzene-d_5. The lines on the graph represent connected dots.

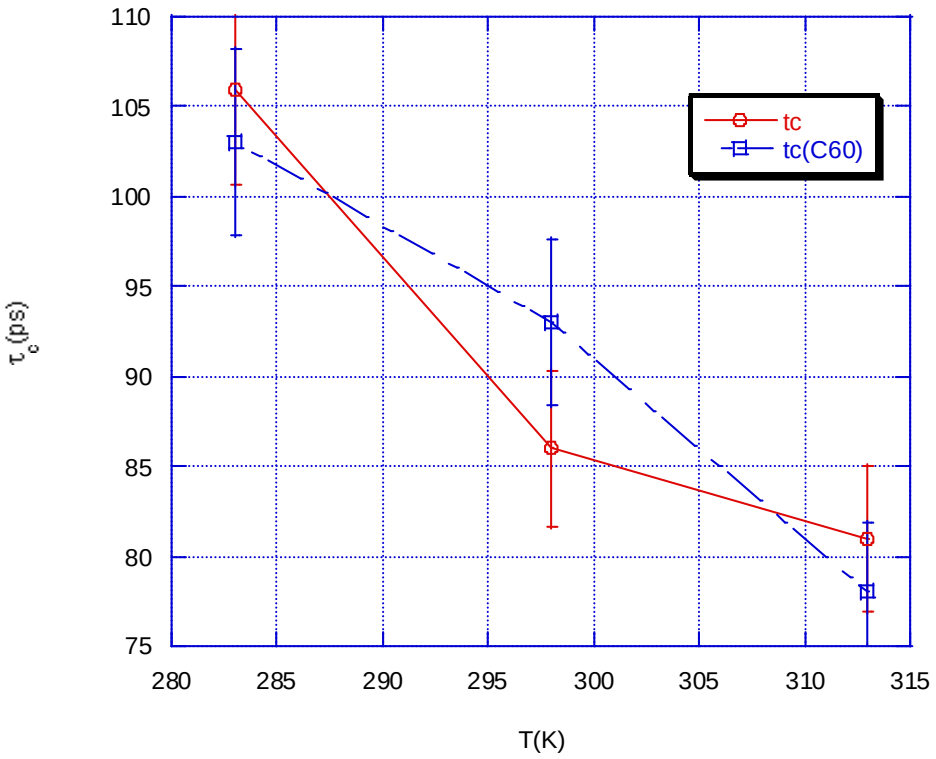

Figure 16. Experimental Correlation times of phenyl hydrogen in H_2[TPP] with C_{60}, R_1 (dashed line) and without C_{60}, R_1C_{60}(Solid line) in chlorobenzene-d_5. The lines on the graph represent connected dots.

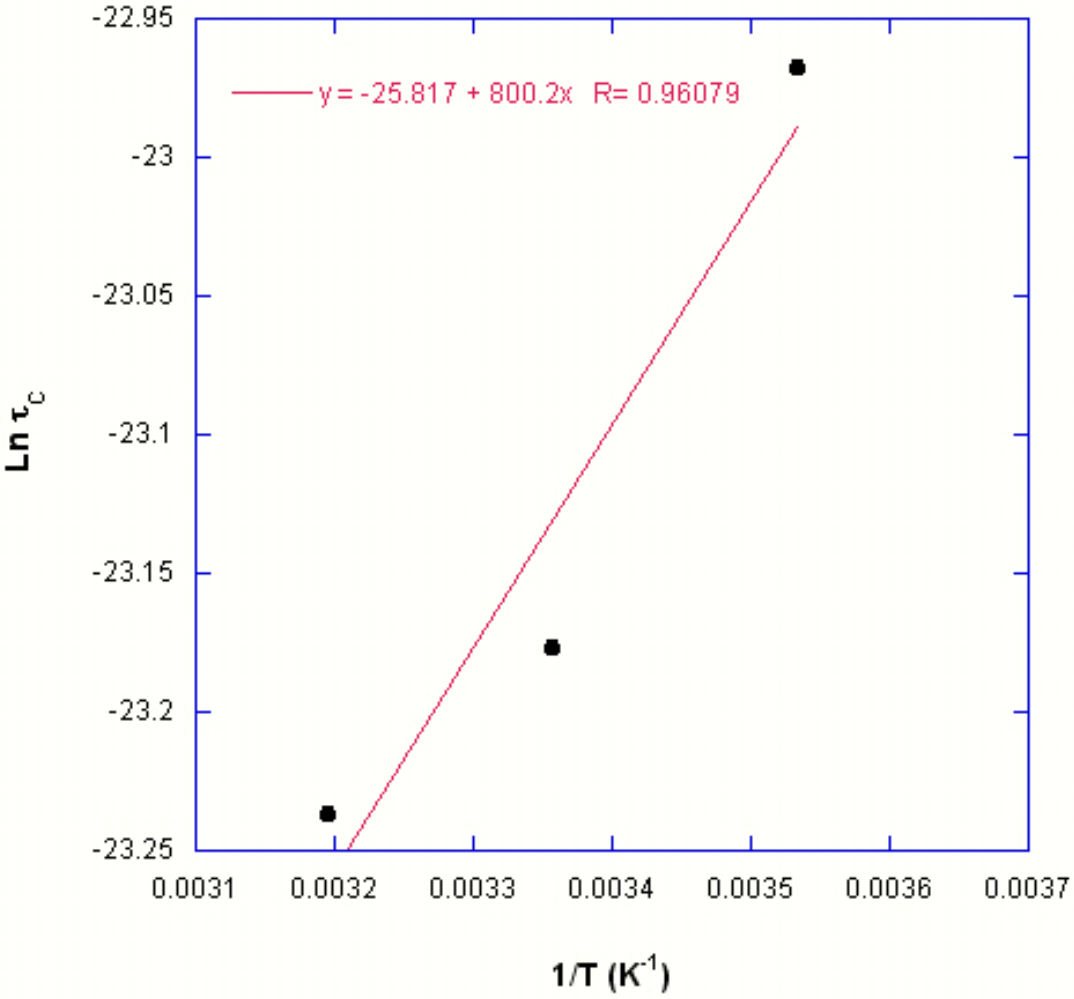

Figure 17. Linear fit of experimental correlation times of the phenyl protons of H_2[TPP] with C_{60}, in neat chlorobnzene-d_5 to obtain activation energy of complexation at the site of interaction.

Overall, our data indicates that there no long-lasting intermolecular interaction between H_2[TPP] and C_{60} in chlorobenzene-d_5 at the pyrrole site where as at the phenyl hydrogen site the results are within the experimental error an indication that the presence of C_{60} does not lead to noticeable intermolecular interaction at the pyrrole site of H_2[TPP].

2.1 ^{1}H Relaxation rates and correlation time of pyrrole hydrogen in $H_2[(p\text{-}OCH_3)_4TPP]$ with and without C_{60} in chlorobenzene-d_5

In column 2 of Table 4, the relaxation rate of the pyrrole hydrogen $H_2[(p\text{-}OCH_3)_4TPP]$ in the absence of C_{60} is given. One sees that the relaxation rate decreases with increasing temperature suggesting that the relaxation pathway is becoming less efficient or less effective as the temperature increases. The effectiveness from the dipole-dipole pathway is inversely proportional to how fast the dynamic motion is at that molecular site. This further illustrated in the correlation time, τ_c. One sees that the correlation time decrease with increasing temperature indicating that the molecule is undergoing faster dynamics with rising temperature.

Column 4 of the same table shows the relaxation rate of the same proton with the introduction of C_{60} into solution. One sees that the relaxation rate is decreasing with rising temperature. This also suggests that the pathway is becoming less efficient at relaxing this hydrogen. We also see that the correlation time decrease with rising temperature which again indicate faster molecular motion.

Interestingly, the introduction of C_{60} to the solution enhances the relaxation rate of this proton as seen in positive values of ΔR. These positive values indicate that the relaxation mechanism (dipole-dipole) is more efficient with the presence of C_{60}. The effectiveness is enhanced because of the slowing down of the dynamic motion of the $H_2[(p\text{-}OCH_3)_4TPP]$ at this site. This indicates that $H_2[(p\text{-}OCH_3)_4TPP]$ is undergoing intermolecular interaction with C_{60} at this site. The temperature behavior of the relaxation rates and correlation times of pyrrole proton with and without C_{60} is illustrated in Figures 18 and 19 respectively.

An Arrhenius fit of τ_c versus 1/T gave values of 2.99 and 2.33 kJ/mole for $H_2[(p\text{-}OCH_3)_4TPP]$ and $H_2[(p\text{-}OCH_3)_4TPP]$ with C_{60}, respectively.

Table 4. ^{1}H Relaxation rates of pyrrole hydrogen in $H_2[(_P\text{-}OCH_3)_4TPP]$with and without C_{60} in chlorobenzene-d_5 (CBZ).

T (K)	$H_2[(_P\text{-}OCH_3)_4TPP]$ in CBZ		$H_2[(_P\text{-}OCH_3)_4TPP]$ with C_{60} in CBZ			
	R_1 (1/s)	τ_C (ps)	R_1 (1/s)	τ_C (ps)	ΔR_1 (1/s)	$\Delta\tau_C$ (ps)
283	0.660 (0.04)	334	0.688 (0.035)	344	0.028	10
298	0.624 (0.045)	316	0.659 (0.062)	333	0.035	17
313	0.584 (0.015)	295	0.618 (0.293)	313	0.034	18

Values in parenthesis are error limits at the 90% confidence limits. Each relaxation time is an average of three measurements.

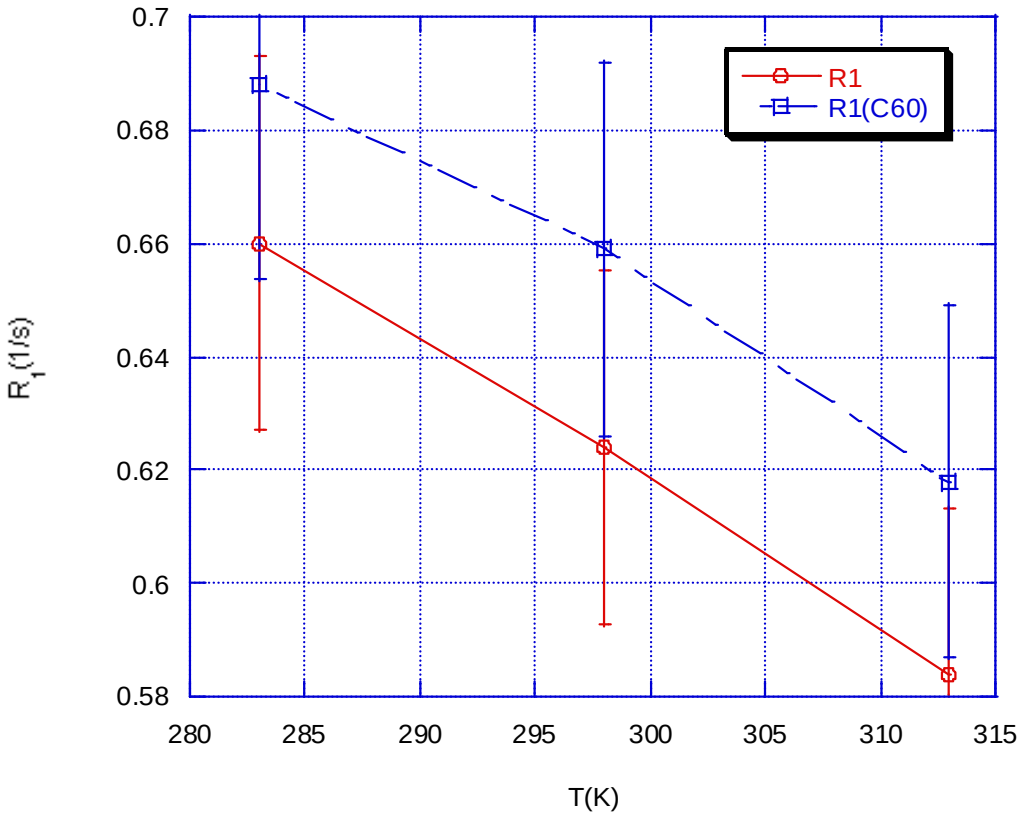

Figure 18. Relaxation rates of pyrrole hydrogen in $H_2[(p\text{-}OCH_3)_4TPP]$ with C_{60}, R_1 (dashed line) and without C_{60}, R_1C_{60}(Solid line) in chlorobenzene-d_5. The lines on the graph represent connected dots.

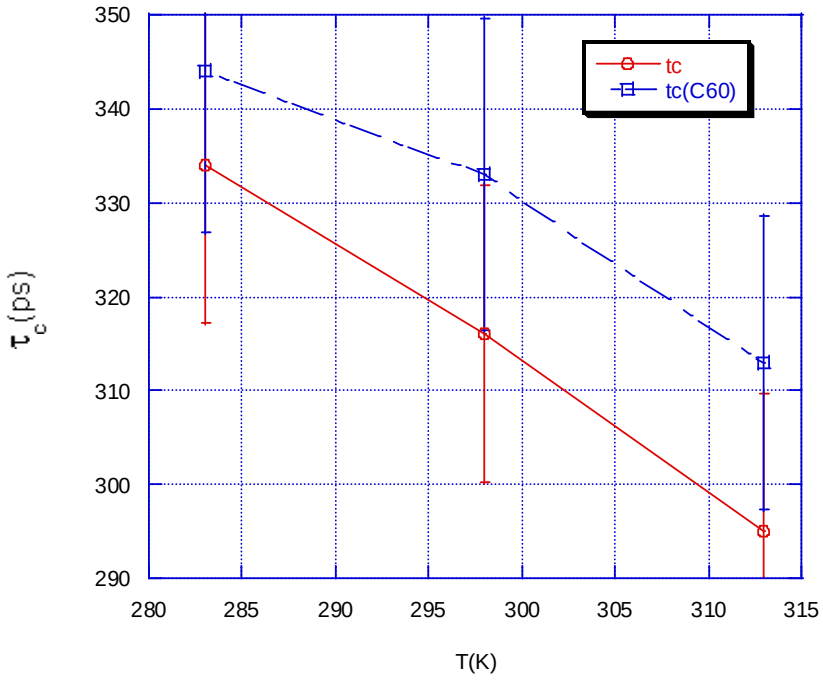

Figure 19. Experimental Correlation times of pyrrole hydrogen in H_2[(p-OCH_3)$_4$TPP] with C_{60}, R_1 (dashed line) and without C_{60}, R_1C_{60}(Solid line) in chlorobenzene-d_5. The lines on the graph represent connected dots.

2.2 ^{1}H Relaxation rates and correlation Time of phenyl hydrogen in $H_2[(p\text{-}OCH_3)_4TPP]$ with and without C_{60} in chlorobenzene-d_5

In column 2 of Table 5, the relaxation rate of the phenyl hydrogen in the absence of C_{60}, is shown. The relaxation rate also is seen to decrease with rising temperature indicating that the dipole-dipole relaxation pathway is becoming less efficient or less effective. As noted earlier the effectiveness from the dipole-dipole pathway is inversely proportional to how fast the dynamic motion is at that molecular site. Further this is shown in the correlation time, τ_c where the correlation time is seen to decrease with increasing temperature indicating that the molecule is undergoing faster dynamics.

In column 4 of the same table shows the relaxation rate of the same hydrogen in the presence of $C_{60.}$ The relaxation rate of this hydrogen is seen to decrease with rising temperature. We also see that the correlation time decrease with rising temperature which again indicates faster molecular motion.

It is noted that the introduction of C_{60} to the solution enhances the relaxation rate of this proton as seen in positive values of ΔR. These positive values indicate that the dipole-dipole relaxation mechanism is more efficient with the presence of C_{60}. The effectiveness is enhanced because of the slowing down of the dynamic motion of the $H_2[(p\text{-}OCH_3)_4TPP]$ as a result of undergoing simultaneous face-to face and face-to- edge π-π interactions between the phenyl moiety and C_{60} . Figure 20 and 21 illustrates the how relaxation rates and correlation times of the phenyl hydrogen varies with the temperature in the presence or absence of C_{60} respectively.

An Arrhenius fit of τ_c versus 1/T gave values of 1.72 and 1.80 kJ/mole for $H_2[(p\text{-}OCH_3)_4TPP]$ and $H_2[(p\text{-}OCH_3)_4TPP]$ with C_{60}, respectively.

Table 5. ^{1}H Relaxation rates of phenyl hydrogen in $H_2[(P\text{-}OCH_3)_4TPP]$ with and without C_{60} in chlorobenzene-d_5 (CBZ).

T (K)	$H_2[(_P\text{-}OCH_3)_4TPP]$ in CBZ		$H_2[(_P\text{-}OCH_3)_4TPP]$ with C_{60} in CBZ			
	R_1 (1/s)	τ_C (ps)	R_1 (1/s)	τ_C (ps)	ΔR_1 (1/s)	$\Delta\tau_C$ (ps)
283	0.660 (0.04)	334	0.688 (0.035)	344	0.028	10
298	0.624 (0.045)	316	0.659 (0.062)	333	0.035	17
313	0.584 (0.015)	295	0.618 (0.293)	313	0.034	18

Values in parenthesis are error limits at the 90% confidence limits. Each relaxation time is an average of three measurements.

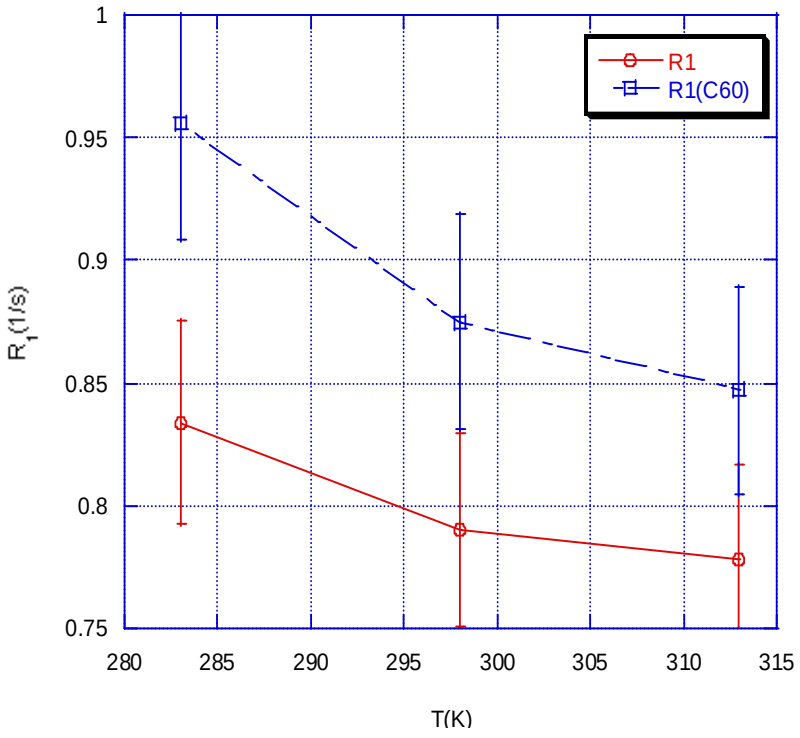

Figure 20. Relaxation rates of phenyl hydrogen in $H_2[(p\text{-}OCH_3)_4TPP]$ with C_{60}, R_1 (dashed line) and without C_{60}, R_1C_{60}(Solid line) in chlorobenzene-d_5. The lines on the graph represent connected dots.

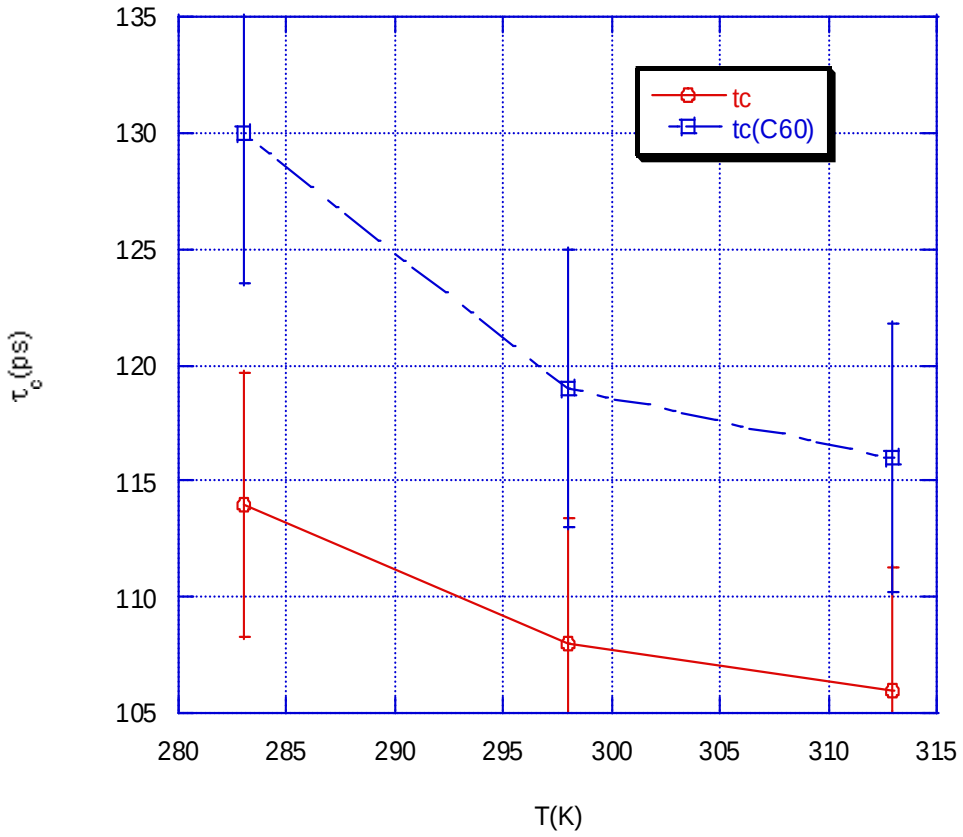

Figure 21. Experimental Correlation times of phenyl hydrogen in H_2[(p-OCH_3)$_4$TPP] with C_{60}, R_1 (dashed line) and without C_{60}, R_1C_{60}(Solid line) in chlorobenzene-d_5. The lines on the graph represent connected dots.

Our data indicates that C_{60} interacts at both the pyrrole and phenyl hydrogen site of_H_2[(p-OCH_3)$_4$TPP]. The values indicate a slight preference for the pyrrole hydrogen site. This is shown in Table 5 where the change in ΔR and $\Delta\tau_c$ at the pyrrole site are more positive or larger than at the phenyl site.

3.1 ^{1}H Relaxation rates and correlation Time of pyrrole hydrogen in H_2[(p-CN)$_4$TPP] with and without C_{60} in chlorobenzene-d_5

The temperature behavior of relaxation rates and correlation times of the pyrrole hydrogen in H_2[(p-CN)$_4$TPP] with and without C_{60} is illustrated in Figures 22 and 23 respectively. Column 2 of Table 6 shows that as the temperature increases the relaxation rate of the pyrrole hydrogen in the absence of C_{60}, is seen to decrease. This implies that the dipole-dipole relaxation pathway is becoming less efficient or less effective as the temperature increases. The effectiveness of the relaxation from the dipole-dipole pathway is inversely proportional to how fast the dynamic motion at that molecular site. The correlation time, τ_c is seen to decrease with increasing temperature indicating the molecule is undergoing faster dynamics with rising temperature.

Column 4 of the same table contains the relaxation rate of the pyrrole hydrogen with C_{60} into solution. One sees that the relaxation rate of the pyrrole hydrogen is decreasing with rising temperature. This also implies that the pathway is becoming less efficient at relaxing this hydrogen. We also see that the correlation time decreasing with rising temperature which again indicates faster molecular motion.

It is worth noticing that, with the introduction of C_{60} to the solution the relaxation rate is enhanced as seen in positive value of ΔR only at the temperature 283ºC. This positive value indicates that the relaxation mechanism (dipole-dipole) is more efficient with the presence of C_{60} at this temperature. As the temperature rises, there is no noticeable interaction indicating that a rise in thermal energy overcomes any long-lasing interactions at this site. An Arrhenius fit of τ_c versus 1/T gave values of 2.99 and 2.33 kJ/mole for H_2[(p-CN)$_4$TPP]and H_2[(p-CN)$_4$TPP] with C_{60}, respectively.

Table 6. ^{1}H Relaxation rates of pyrrole hydrogen in $H_2[(_P\text{-}CN)_4TPP]$ with and without C_{60} in chlorobenzene-d_5 (CBZ).

T (K)	$H_2[(p\text{-}CN)_4TPP]$		$H_2[(_P\text{-}CN)_4TPP]$ with C_{60}			
	R_1 (1/s)	τ_C (ps)	R_1 (1/s)	τ_C (ps)	ΔR_1 (1/s)	$\Delta\tau_C$ (ps)
283	0.820 (0.0625)	415	0.878 (0.147)	444	0.058	29
298	0.813 (0.094)	418	0.781 (0.021)	395	-0.032	-23
313	0.809 (0.050)	455	0.765 (0.090)	403	-0.044	-52

Values in parenthesis are error limits at the 90% confidence limits. Each relaxation time is an average of three measurements.

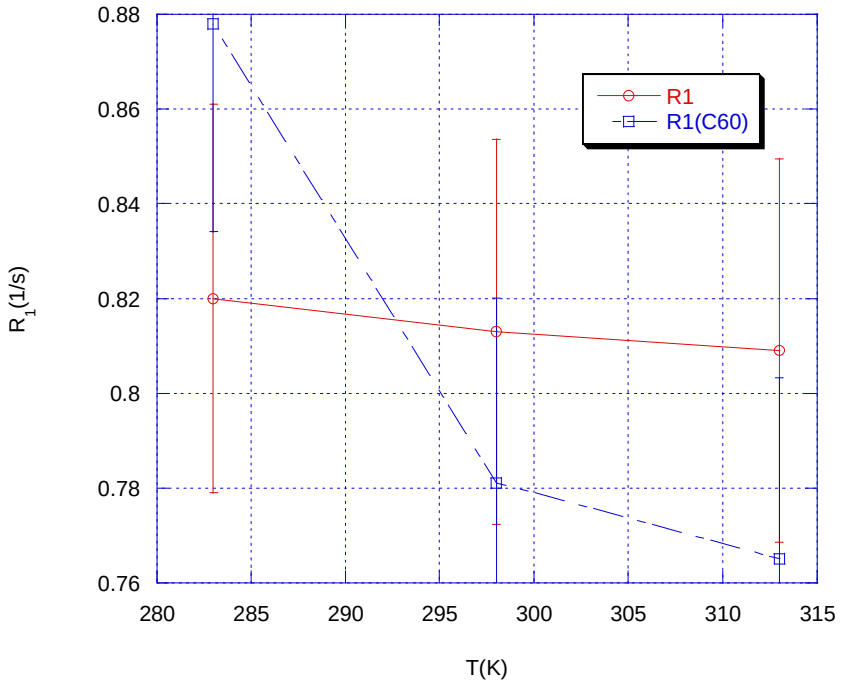

Figure 22. Relaxation rates of pyrrole hydrogen in $H_2[(p\text{-}CN)_4TPP]$ with C_{60}, R_1 (dashed line) and without C_{60}, R_1C_{60} (Solid line) in chlorobenzene-d_5. The lines on the graph represent connected dots.

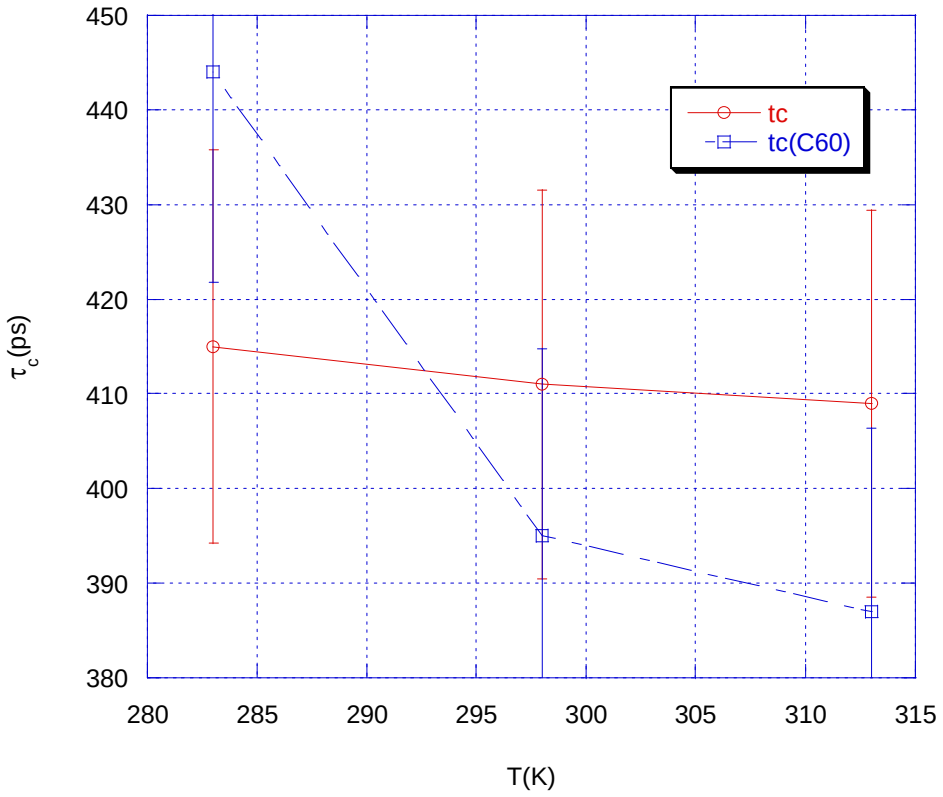

Figure 23. Experimental correlation times of pyrrole hydrogen in H_2[(p-CN)$_4$TPP] with C_{60}, R_1 (dashed line) and without C_{60}, R_1C_{60}(Solid line) in chlorobenzene-d_5. The lines on the graph represent connected dots.

3.2 ^{1}H Relaxation rates and correlation Time of phenyl hydrogen in $H_2[(_p\text{-}CN)_4TPP]$ with and without C_{60} in chlorobenzene-d_5

The relaxation rate of the phenyl hydrogen of $H_2[(p\text{-}CN)_4TPP]$ in the absence of C_{60} shown in column 2 of Table 7. As seen in this table, the relaxation rate decreases with rising temperature suggesting that the relaxation pathway is becoming less efficient or less effective. This is further shown in the correlation time, τ_c. Correlation time is decreasing with increasing temperature indicated that the molecule is undergoing faster dynamics with rising temperature. These observations are also illustrated in Figure 24.

Column 4 of the same table contains the relaxation rate of the same proton in presence of C_{60} in solution. One sees that the relaxation rate decreases with rising temperature suggesting that the pathway is becoming less efficient at relaxing this hydrogen. We also see that the correlation time decrease with rising temperature which again indicate faster molecular motion.

The relaxation rate of this proton is seen to be enhanced with the introduction of C_{60} to the solution as reflected in the positive values of ΔR at the temperature 283 K. This positive value indicates that the relaxation mechanism (dipole-dipole) is more efficient with the presence of C_{60}. As the temperature rises there is no noticeable interaction indicating that rise in thermal energy overcomes any long lasting interaction at this site.

An Arrhenius fit of τ_c versus 1/T gave values of 2.40 and 2.30 kJ/mole for $H_2[(p\text{-}CN)_4TPP]$ and $H_2[(p\text{-}CN)_4TPP]$ with C_{60}, respectively

Table 7. ^{1}H Relaxation rates of phenyl hydrogen in H_2[(p-CN)$_4$TPP]with and without C_{60} in chlorobenzene-d_5 (CBZ).

T (K)	H_2[($_P$-CN)$_4$TPP]		H_2[(P-CN)$_4$TPP] with C_{60}			
	R_1 (1/s)	τ_C (ps)	R_1 (1/s)	τ_C (ps)	ΔR_1 (1/s)	$\Delta\tau_C$ (ps)
283	0.968 (0.152)	136	0.986 (0.236)	139	0.018	3
298	0.913 (0.260)	128	0.838 (0.037)	118	-0.075	-10
313	0.879 (0.161)	185	0.832 (0.129)	131	-0.385	-54

Values in parenthesis are error limits at the 90% confidence limits. Each relaxation time is an average of three measurements. The lines on the graph represent connected dots.

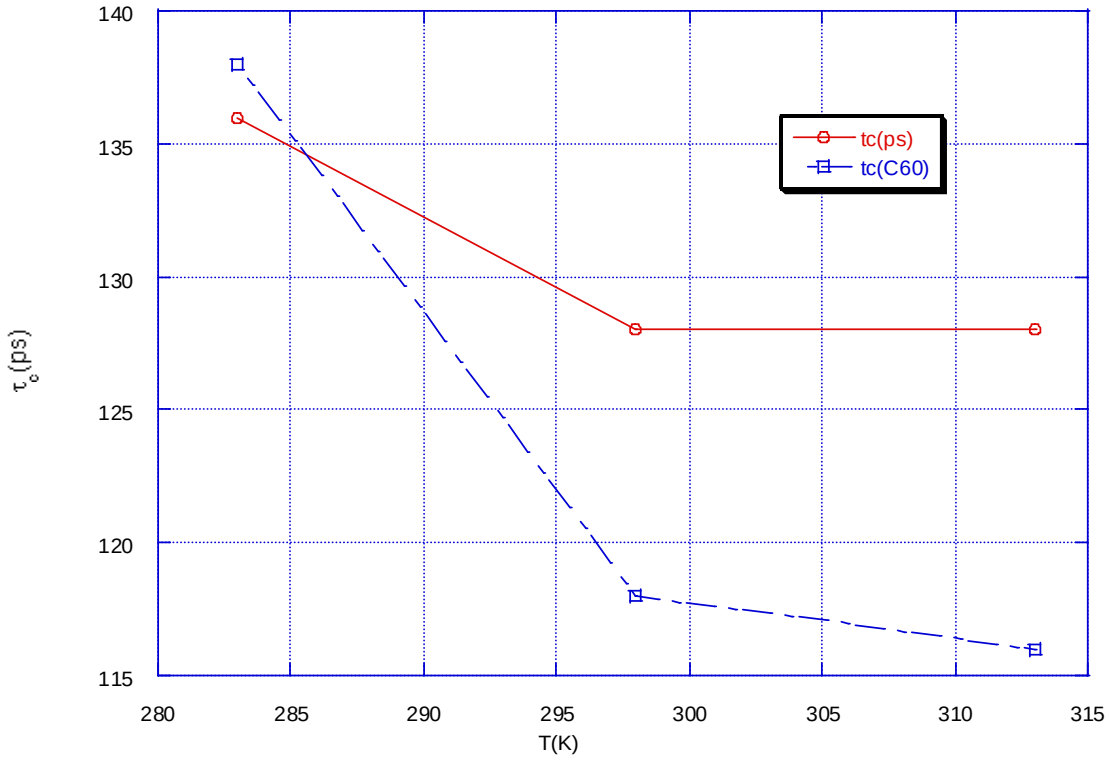

Figure 24. Experimental correlation times of phenyl hydrogen in H_2[(p-CN)$_4$TPP] with C_{60}, R_1 (dashed line) and without C_{60}, R_1C_{60} (Solid line) in toluene-d_8. The lines on the graph represent connected dots.

In H_2[(p-CN)$_4$TPP] porhyrin derivative, our data indicates that at lower temperature (283 K) there is a slight preference for interaction of C_{60} at the pyrrole site but is quickly destroyed with increase in temperature.

4.1 ^{1}H Relaxation rates and correlation Time of pyrrole hydrogen in H_2[TPP] with and without C_{60} in toluene-d_8

In order to investigate the possible role that a solvent can play on interaction, the relaxation rates of the pyrrole and phenyl hydrogen were done in toluene-d_8. In Table 8, column 2 and 4 shows the relaxation rates of the pyrrole hydrogen of H_2[TPP] without and with C_{60} respectively. One sees a small increase in the relaxation rates at all the temperatures. Increasing relaxation rates indicates slower dynamical motion at that site which is also reflected in the longer correlation times, τ_C, that is observed when C_{60} is added to the solution. Figure 25 and 26 also illustrates the temperature behavior of relaxation rates and correlation times with and without C_{60} being in solution respectively. These changes are indicating that C_{60} may be interacting at this site.

Table 8. ^{1}H Relaxation rates of pyrrole hydrogen in H_2[TPP] with and without C_{60} in toluene-d_8.

T (K)	H_2 [TPP] in Toluene		H_2[TPP] with C_{60} in Toluene			
	R_1 (1/s)	τ_C (ps)	R_1 (1/s)	τ_C (ps)	ΔR_1 (1/s)	$\Delta\tau_C$ (ps)
283	0.518 (0.005)	256	0.523 (0.002)	259	0.005	3
298	0.432 (0.010)	214	0.444 (0.002)	220	0.012	6
313	0.363 (0.001)	180	0.374 (0.003)	185	0.011	5

Values in parenthesis are error limits at the 90% confidence limits. Each relaxation time is an average of three measurements.

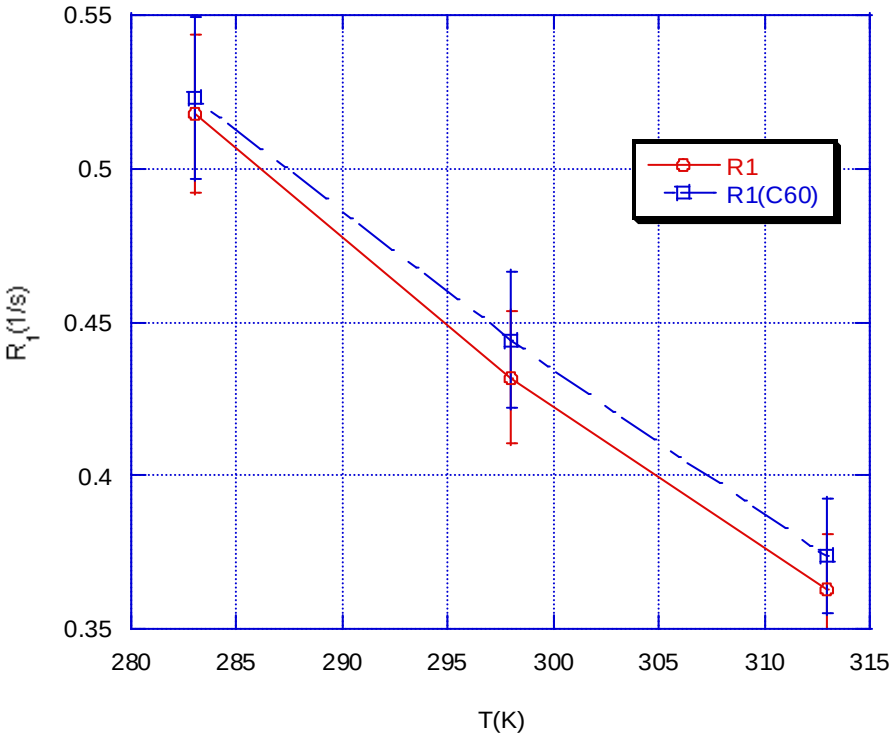

Figure 25. Relaxation rates of pyrrole hydrogen in H_2TPP with C_{60}, R_1 (dashed line) and without C_{60}, R_1C_{60} (Solid line) in toluene-d_8. The lines on the graph represent connected dots.

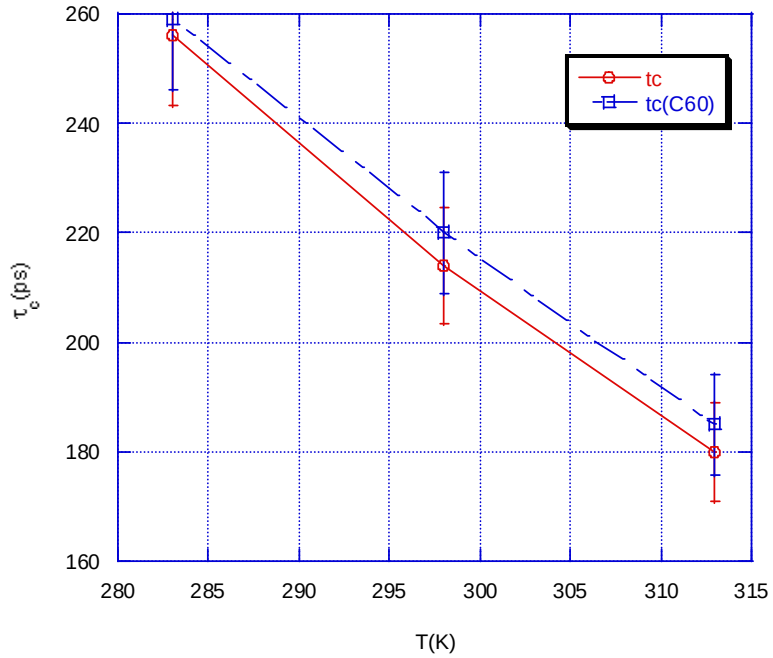

Figure 26. Experimental correlation times of pyrrole hydrogen in H_2TPP] with C_{60}, R_1 (dashed line) and without C_{60}, R_1C_{60} (Solid line) in toluene-d_8. The lines on the graph represent connected dots.

4.2 ^{1}H Relaxation rates and correlation Time of phenyl hydrogen in H_2[TPP] with and without C_{60} in toluene-d_8

In column 2 of Table 9 contains the relaxation rate of the phenyl hydrogen in the absence of C_{60}.The relaxation rate are seen to decrease with rising temperature indicating that the relaxation pathway is becoming less efficient or less effective. The correlation time is seen to decrease with increasing temperature indicating that the molecule is undergoing faster dynamics with rising temperature. An illustration showing the variation of relaxation rate and correlation times of the phenyl hydrogen with temperature in absence and presence of C_{60} is shown in Figures 27 and 28.

Column 4 shows the relaxation rates of the same hydrogen with the introduction of C_{60} into solution. It is shown that that the relaxation rate decreases with rising temperature. We also see that the correlation time decrease with rising temperature which again indicate faster molecular motion.

Table 9. ^{1}H Relaxation rates of phenyl hydrogen in H_2[TPP] with and without C_{60} in toluene-d_8.

T (K)	H_2[TPP] in Toluene		H_2[TPP] with C_{60} in Toluene			
	R_1 (1/s)	τ_C (ps)	R_1 (1/s)	τ_C (ps)	ΔR_1 (1/s)	$\Delta\tau_C$ (ps)
283	0.674 (0.009)	95	0.677 (0.005)	96	0.006	1
298	0.578 (0.017)	82	0.574 (0.003)	-4	0.004	-1
313	0.469 (0.013)	66	0.483 (0.004)	68	0.014	2

Values in parenthesis are error limits at the 90% confidence limits. Each relaxation time is an average of three measurements.

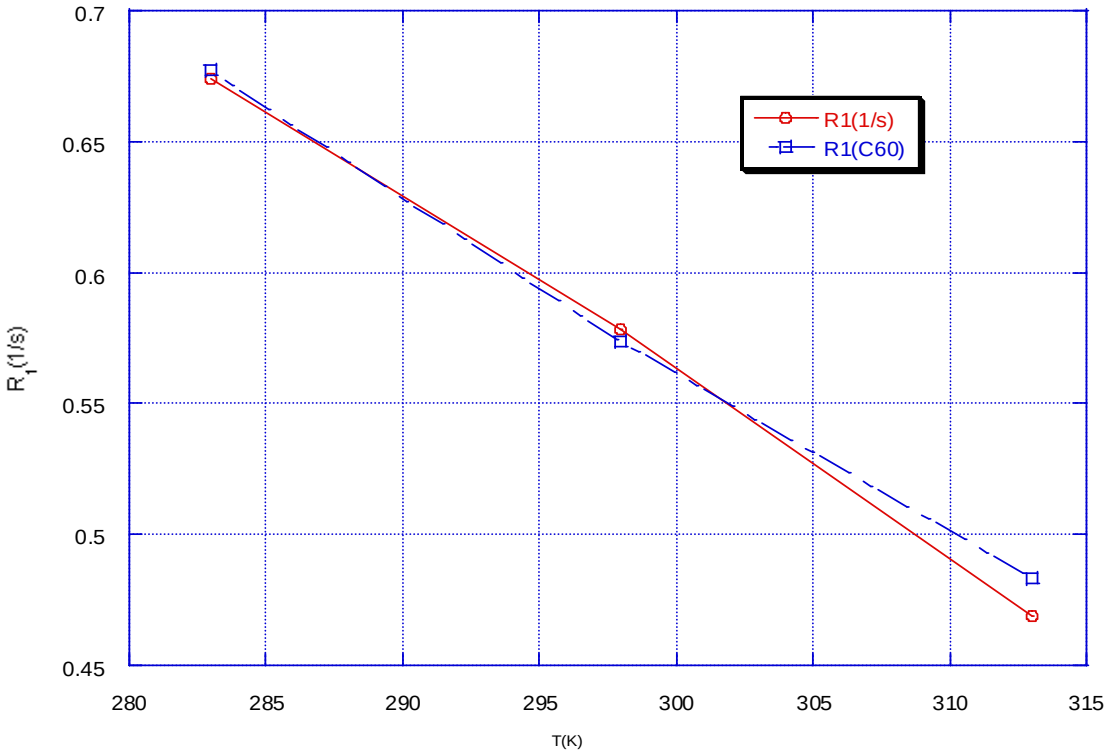

Figure 27. Relaxation rates of phenyl hydrogen in H_2[TPP] with C_{60}, R_1 (dashed line) and without C_{60}, R_1C_{60} (Solid line) in toluene-d_8. The lines on the graph represent connected dots.

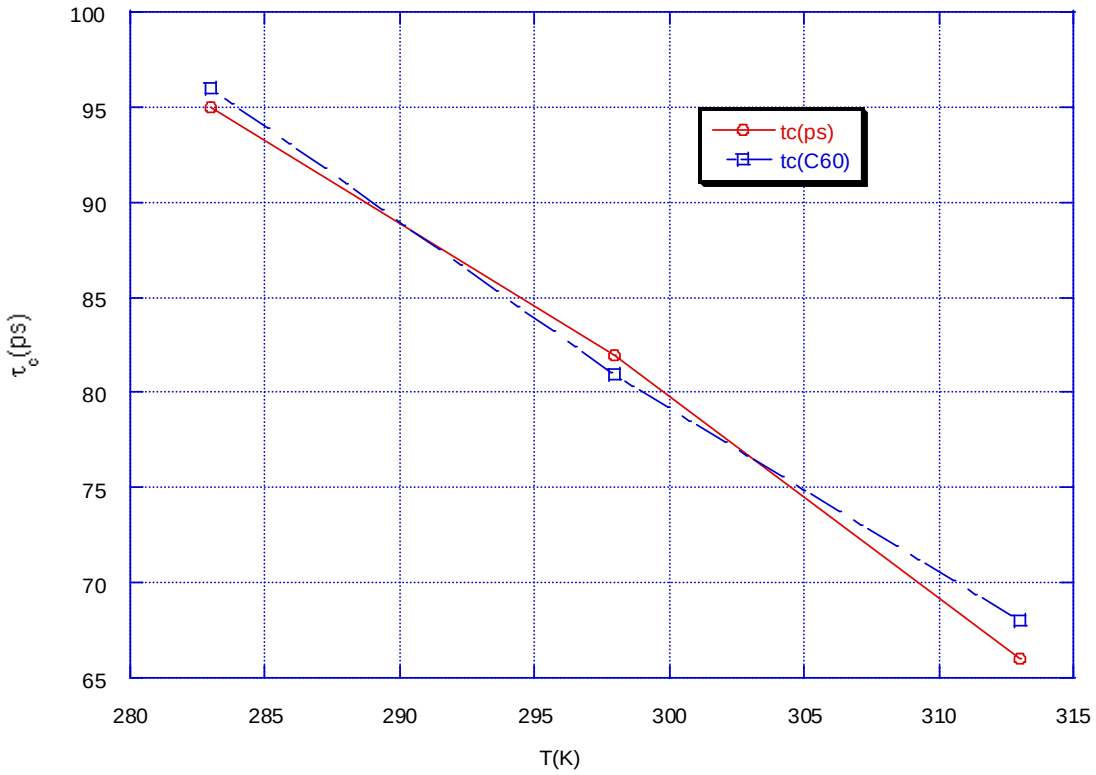

Figure 28. Experimental correlation times of phenyl hydrogen in H_2[TPP] with C_{60}, R_1 (dashed line) and without C_{60}, R_1C_{60} (Solid line) in toluene-d_8. The lines on the graph represent connected dots.

Although the introduction of C_{60} to the solution enhances the relaxation rate of this proton, as seen in positive values of ΔR, the relaxation rates for this hydrogen are within experimental error and are inconclusive suggesting that there is little or no intermolecular interaction at this site.

CONCLUSIONS

1. Our data indicates that the introduction of C_{60} in solution of H_2[TPP] does not lead to noticeable intermolecular interaction at both the pyrrole and phenyl hydrogen sites of H2[TPP] since the interactions are not long-lasting in chlorobenzene-d_5.
2. Our data indicates that C_{60} interacts at both the pyrrole and phenyl hydrogen site of H_2[(P-OCH_3)$_4$TPP], with a slight preference for the pyrrole hydrogen site.
3. For the complex H_2[(P-CN)$_4$TPP], our data indicates that at lower temperature there is a noticeable but slight preference for the interaction of C_{60} at pyrrole site at lower temperature(283 K), but is quickly destroyed with an increase in temperature.
4. The porphyrin derivatives show that the substituents have an effect on interaction site due to a change in substituent. For the case of H_2[(p-OCH_3)$_4$TPP], that has an electron – donating group, OCH_3 both phenyl and pyrrole hydrogen sites are seen to interact with C_{60}, with a slight preference at the pyrrole hydrogen at all the three temperatures(283, 298, and 313ºC). In the case of H_2[(p-CN)$_4$TPP] with an electron-withdrawing group CN, only at lower temperature(283 K) does the pyrrole hydrogen site interact with C_{60}.

REFERENCES

(1) Boyd Peter, D. W.; Reed, C. A. Fullerene-Porphyrin Constructs. *Acc. Chem. Res.* 2005, *38*, 235-242.

(2) Balch, A. L.; Olmstead, M. M. Structural Chemistry of Supramolecular Assemblies that Place Flat Molecular Surfaces Around the Curved Exteriors of Fullerenes. *Coord. Chem. Rev.* 1999, *185-186*, 601-617.

(3) Sun, D.; Tham, F. S.; Reed, C. A.; Chaker, L.; Boyd, P. D. W. Supramolecular Fullerene-Porphyrin Chemistry. Fullerene Complexation by Metalated "Jaws Porphyrin" Hosts. *J. Am. Chem. Soc.* 2002, *124*, 6604-6612.

(4) Boyd, P. D. W.; Hodgson, M. C.; Rickard, C. E. F.; Oliver, A. G.; Chaker, L.; Brothers, P. J.; Bolskar, R. D.; Tham, F. S.; Reed, C. A. Selective Supramolecular Porphyrin/Fullerene Interactions. *J. Am. Chem. Soc.* 1999, *121*, 10487-10495.

(5) Sessler J. L.; Jayawickramarajah J.; Gouloumis A.; Torres T.; Guldi D. M.; Maldonado S.; Stevenson K. J.
Synthesis and Photophysics of a porphyrin–fullerene Dyad Assembled
through Watson–Crick Hydrogen Bonding. *Chem. Commun. (Cambridge, U. K.)* 2005, , 1892.

(6) D'Souza, F.; Deviprasad, G. R.; Zandler, M. E.; El-Khouly, M. E.; Fujitsuka, M.; Ito, O. Photoinduced Electron Transfer in "Two-Point" Bound Supramolecular Triads Composed of N,N-Dimethylaminophenyl-Fullerene-Pyridine Coordinated to Zinc Porphyrin. *J. Phys. Chem. A* 2003, *107*, 4801-4807.

(7) Solladie, N.; Walther, M. E.; Gross, M.; Figueira Duarte, T. M.; Bourgogne, C.; Nierengarten, J. A Supramolecular Cup-and-Ball C60-Porphyrin Conjugate System. *Chem. Commun. (Cambridge, U. K.)* 2003, , 2412-2413.

(8) Yoshimoto, S.; Honda, Y.; Murata, Y.; Murata, M.; Komatsu, K.; Ito, O.; Itaya, K. Dependence of Molecular Recognition of Fullerene Derivative on the Adlayer Structure of Zinc Octaethylporphyrin Formed on Au(100) Surface. *J. Phys. Chem. B* 2005, *109*, 8547-8550.

(9) Jiang, D.; Aida, T. Bioinspired Molecular Design of Functional Dendrimers. *Prog. Polym. Sci.* 2005, *30*, 403-422.

(10) D'Souza, F.; Smith, P. M.; Zandler, M. E.; McCarty, A. L.; Itou, M.; Araki, Y.; Ito, O. Energy Transfer Followed by Electron Transfer in a Supramolecular Triad Composed of Boron Dipyrrin, Zinc Porphyrin, and Fullerene: A Model for the Photosynthetic Antenna-Reaction Center Complex. *J. Am. Chem. Soc.* 2004, *126*, 7898-7907.

(11) Imahori, H. Porphyrin-Fullerene Linked Systems as Artificial Photosynthetic Mimics. *Org. Biomol. Chem.* 2004, *2*, 1425-1433.

(12) Gust, D.; Moore, T. A.; Moore, A. L. Mimicking Photosynthetic Solar Energy Transduction. *Acc. Chem. Res.* 2001, *34*, 40-48.

(13) Imahori, H.; Norieda, H.; Yamada, H.; Nishimura, Y.; Yamazaki, I.; Sakata, Y.; Fukuzumi, S. Light-Harvesting and Photocurrent Generation by Gold Electrodes Modified with Mixed Self-Assembled Monolayers of Boron-Dipyrrin and Ferrocene-Porphyrin-Fullerene Triad. *J. Am. Chem. Soc.* 2001, *123*, 100-110.

(14) Cho, Y.; Ahn, T. K.; Song, H.; Kim, K. S.; Lee, C. Y.; Seo, W. S.; Lee, K.; Kim, S. K.; Kim, D.; Park, J. T. Unusually High Performance Photovoltaic Cell Based on a [60]Fullerene Metal Cluster-Porphyrin Dyad SAM on an ITO Electrode. *J. Am. Chem. Soc.* 2005, *127*, 2380-2381.

(15) Hasobe, T.; Imahori, H.; Kamat, P. V.; Ahn, T. K.; Kim, S. K.; Kim, D.; Fujimoto, A.; Hirakawa, T.; Fukuzumi, S. Photovoltaic Cells using Composite Nanoclusters of Porphyrins and Fullerenes with Gold Nanoparticles. *J. Am. Chem. Soc.* 2005, *127*, 1216-1228.

(16) Imahori, H.; Kimura, M.; Hosomizu, K.; Sato, T.; Ahn, T. K.; Kim, S. K.; Kim, D.; Nishimura, Y.; Yamazaki, I.; Araki, Y.; Ito, O.; Fukuzumi, S. Vectorial Electron Relay at ITO Electrodes Modified with Self-Assembled Monolayers of Ferrocene-Porphyrin-Fullerene Triads and Porphyrin-Fullerene Dyads for Molecular Photovoltaic Devices. *Chem. --Eur. J.* 2004, *10*, 5111-5122.

(17) Hasobe, T.; Hattori, S.; Kotani, H.; Ohkubo, K.; Hosomizu, K.; Imahori, H.; Kamat, P. V.; Fukuzumi, S. Photoelectrochemical Properties of Supramolecular Composite of Fullerene Nanoclusters and 9-Mesityl-10-Carboxymethylacridinium Ion on SnO2. *Org. Lett.* 2004, *6*, 3103-3106.

(18) Imahori, H.; Fukuzumi, S. Porphyrin- and Fullerene-Based Molecular Photovoltaic Devices. *Adv. Funct. Mater.* 2004, *14*, 525-536.

(19) Yamada, H.; Imahori, H.; Nishimura, Y.; Yamazaki, I.; Ahn, T. K.; Kim, S. K.; Kim, D.; Fukuzumi, S. Photovoltaic Properties of Self-Assembled Monolayers of Porphyrins and Porphyrin-Fullerene Dyads on ITO and Gold Surfaces. *J. Am. Chem. Soc.* 2003, *125*, 9129-9139.

(20) Nierengarten, J. -.; Eckert, J. -.; Felder, D.; Nicoud, J. -.; Armaroli, N.; Marconi, G.; Vicinelli, V.; Boudon, C.; Gisselbrecht, J. -.; Gross, M.; Hadziioannou, G.; Krasnikov, V.; Ouali, L.; Echegoyen, L.; Liu, S. -. Synthesis and Electronic Properties of Donor-Linked Fullerenes Towards Photochemical Molecular Devices. *Carbon* 2000, *38*, 1587-1598.

(21) Guldi, D. M.; Imahori, H.; Tamaki, K.; Kashiwagi, Y.; Yamada, H.; Sakata, Y.; Fukuzumi, S. A Molecular Tetrad Allowing Efficient Energy Storage for 1.6 s at 163 K. *J. Phys. Chem. A* 2004, *108*, 541-548.

(22) Guldi, D. M.; Da Ros, T.; Braiuca, P.; Prato, M.; Alessio, E. C60 in the Box. A Supramolecular C60-Porphyrin Assembly. *J. Mater. Chem.* 2002, *12*, 2001-2008.

(23) Kodis, G.; Liddell, P. A.; de la Garza, L.; Clausen, P. C.; Lindsey, J. S.; Moore, A. L.; Moore, T. A.; Gust, D. Efficient Energy Transfer and Electron Transfer in an Artificial Photosynthetic Antenna-Reaction Center Complex. *J. Phys. Chem. A* 2002, *106*, 2036-2048.

(24) Da Ros, T.; Prato, M.; Guldi, D. M.; Ruzzi, M.; Pasimeni, L. Efficient Charge Separation in Porphyrin-Fullerene-Ligand Complexes. *Chem. --Eur. J.* 2001, *7*, 816-827.

(25) Gust, D.; Moore, T. A.; Moore, A. L. Photochemistry of Supramolecular Systems Containing C60. *J. Photochem. Photobiol. , B* 2000, *58*, 63-71.

(26) Guldi, D. M.; Torres-Garcia, G.; Mattay, J. Intramolecular Energy Transfer in Fullerene Pyrazine Dyads. *J. Phys. Chem. A* 1998, *102*, 9679-9685.

(27) Kuciauskas, D.; Lin, S.; Seely, G. R.; Moore, A. L.; Moore, T. A.; Gust, D.; Drovetskaya, T.; Reed, C. A.; Boyd, P. D. W. Energy and Photoinduced Electron Transfer in Porphyrin-Fullerene Dyads. *J. Phys. Chem.* 1996, *100*, 15926-15932.

(28) Kutzki, O.; Walter, A.; Montforts, F. Synthesis of Sulfolenobilins and their Cyclization Directed to Chlorinatozinc-Fullerene Dyads. *Helv. Chim. Acta* 2000, *83*, 2231-2245.

(29) Konarev, D. V.; Lyubovskaya, R. N.; Drichko, N. V.; Yudanova, E. I.; Shul'ga, Y. M.; Litvinov, A. L.; Semkin, V. N.; Tarasov, B. P. Donor-Acceptor Complexes of Fullerene C60 with Organic and Organometallic Donors. *J. Mater. Chem.* 2000, *10*, 803-818.

(30) El-Khouly, M. E.; Ito, O.; Smith, P. M.; D'Souza, F. Intermolecular and Supramolecular Photoinduced Electron Transfer Processes of Fullerene-porphyrin/phthalocyanine Systems. *J. Photochem. Photobiol. , C* 2004, *5*, 79-104.

(31) Kesti, T. J.; Tkachenko, N. V.; Vehmanen, V.; Yamada, H.; Imahori, H.; Fukuzumi, S.; Lemmetyinen, H. Exciplex Intermediates in Photoinduced Electron Transfer of Porphyrin-Fullerene Dyads. *J. Am. Chem. Soc.* 2002, *124*, 8067-8077.

(32) Vehmanen, V.; Tkachenko, N. V.; Imahori, H.; Fukuzumi, S.; Lemmetyinen, H. Charge-Transfer Emission of Compact Porphyrin-Fullerene Dyad Analyzed by Marcus Theory of Electron-Transfer. *Spectrochim. Acta, Part A* 2001, *57A*, 2229-2244.

(33) Imahori, H.; Sekiguchi, Y.; Kashiwagi, Y.; Sato, T.; Araki, Y.; Ito, O.; Yamada, H.; Fukuzumi, S. Long-Lived Charge-Separated State Generated in a Ferrocene-Meso,Meso-Linked Porphyrin Trimer-Fullerene Pentad with a High Quantum Yield. *Chem. --Eur. J.* 2004, *10*, 3184-3196.

(34) Sandanayaka, A. S. D.; Sasabe, H.; Araki, Y.; Furusho, Y.; Ito, O.; Takata, T. Photoinduced Electron-Transfer Processes between [C60]Fullerene and Triphenylamine Moieties Tethered by Rotaxane Structures. through-Space Electron Transfer Via Excited Triplet States of [60]Fullerene. *J. Phys. Chem. A* 2004, *108*, 5145-5155.

(35) Ramos, A. M.; Meskers, S. C. J.; van Hal, P. A.; Knol, J.; Hummelen, J. C.; Janssen, R. A. J. Photoinduced Multistep Energy and Electron Transfer in an Oligoaniline-Oligo(p-Phenylene Vinylene)-Fullerene Triad. *J. Phys. Chem. A* 2003, *107*, 9269-9283.

(36) Guldi, D. M.; Hirsch, A.; Scheloske, M.; Dietel, E.; Troisi, A.; Zerbetto, F.; Prato, M. Modulating Charge-Transfer Interactions in Topologically Different Porphyrin-C60 Dyads. *Chem. --Eur. J.* 2003, *9*, 4968-4979.

(37) Ha, J.; Cho, H. S.; Kim, D.; Lee, J.; Kim, T.; Shim, Y. K. Time-Resolved Spectroscopic Study on Photoinduced Electron-Transfer Processes in Zn(II)Porphyrin-Zn(II)Chlorin-Fullerene Triad. *Chemphyschem* 2003, *4*, 951-958.

(38) Ohta, N.; Mikami, S.; Iwaki, Y.; Tsushima, M.; Imahori, H.; Tamaki, K.; Sakata, Y.; Fukuzumi, S. Acceleration and Deceleration of Photoinduced Electron Transfer Rates by an Electric Field in Porphyrin-Fullerene Dyads. *Chem. Phys. Lett.* 2002, *368*, 230-235.

(39) Tkachenko, N. V.; Rantala, L.; Tauber, A. Y.; Helaja, J.; Hynninen, P. H.; Lemmetyinen, H. Photoinduced Electron Transfer in Phytochlorin-[60]Fullerene Dyads. *J. Am. Chem. Soc.* 1999, *121*, 9378-9387.

(40) Fukuzumi, S.; Mori, H.; Imahori, H.; Suenobu, T.; Araki, Y.; Ito, O.; Kadish, K. M. Scandium Ion-Promoted Photoinduced Electron-Transfer Oxidation of Fullerenes and Derivatives by p-Chloranil and p-Benzoquinone. *J. Am. Chem. Soc.* 2001, *123*, 12458-12465.

(41) Welch, C. J.; Pirkle, W. H. Progress in the Design of Selectors for Buckminsterfullerene. *J. Chromatogr.* 1992, *609*, 89-101.

(42) Kimata, K.; Hosoya, K.; Araki, T.; Tanaka, N. [2-(1-Pyrenyl)Ethyl]Silyl Silica Packing Material for Liquid Chromatographic Separation of Fullerenes. *J. Org. Chem.* 1993, *58*, 282-283.

(43) Xiao, J.; Meyerhoff, M. E. High-Performance Liquid Chromatography of C_{60}, C_{70}, and Higher Fullerenes on Tetraphenylporphyrin-Silica Stationary Phases using Strong Mobile Phase Solvents. *J. Chromatogr. , A* 1995, *715*, 19-29.

(44) Sun, Y.; Drovetskaya, T.; Bolskar, R. D.; Bau, R.; Boyd, P. D. W.; Reed, C. A. Fullerides of Pyrrolidine-Functionalized C60. *J. Org. Chem.* 1997, *62*, 3642-3649.

(45) Nelson, J. H. In *Nuclear Magnetic Resonance Spectroscopy;* Prentice Hall: 2003; .

(46) Keeler James In *Understanding NMR Spectroscopy;* John Wiley & Sons Ltd.: West Sussex England, 2005; , pp 476.

(47) Bratoz, S.; Rios, J.; Guissani, Y. Infrared Study of Liquids. I. Theory of the Ir Spectra of Diatomic Molecules in Inert Solutions. *J. Chem. Phys.* 1970, *52*, 439-453.

(48) Tanabe, K.; Hiraishi, J. Raman Study of Vibrational and Reorientational Relaxation of Chloroform in Solution. *Adv. Mol. Relaxation Interact. Processes* 1980, *16*, 281-297.

(49) Abragam A. In *The Principles of Nuclear Magnetism;* Oxford University Press: Oxford, UK, 1983; , pp 648.

(50) Van Woerkom, P. C. M.; De Bleyser, J.; De Zwart, M.; Leyte, J. C. Intermolecular Vibrational Relaxation in Liquids. *Chem. Phys.* 1974, *4*, 236-248.

(51) Huntress, W. T. Anisotropic rotation of molecules in liquid by NMR quadrupolar relaxation *Adv.Magn. Resonance,* 1970, 4, 1-37

(52) Bovey, F. A. In *Nuclear Magnetic Resonance Spectroscopy;* Academic Press: San Diego, California, 1988; .

(53) Acros Organics, 500 American Road, Morris Plain, NJ 07950, USA, http://www.acros.com/, 800-766-7000.

(54) Aldrich Chemical, P. O. Box 14508, Saint Louis, MO 63178, USA, http://www.sigmaaldrich.com/, 800-325-3010.

(55) Adler, A. D.; Longo, F. R.; Finarelli, J. D.; Goldmacher, J.; Assour, J.; Korsakoff, L. A Simplified Synthesis for Meso-Tetraphenylporphine. *J. Org. Chem.* 1967, *32*, 476.